NASA TECHNICAL MEMORANDUM

NASA TM X-1623

NASA TM X-1623

FLIGHT TEST OF A 40-FOOT-NOMINAL-DIAMETER DISK-GAP-BAND PARACHUTE DEPLOYED AT A MACH NUMBER OF 2.72 AND A DYNAMIC PRESSURE OF 9.7 POUNDS PER SQUARE FOOT

by Clinton V. Eckstrom and John S. Preisser

Langley Research Center
Langley Station, Hampton, Va.

NATIONAL AERONAUTICS AND SPACE ADMINISTRATION • WASHINGTON, D. C. • AUGUST 1968

NASA TM X-1623

FLIGHT TEST OF A 40-FOOT-NOMINAL-DIAMETER DISK-GAP-BAND PARACHUTE DEPLOYED AT A MACH NUMBER OF 2.72 AND A DYNAMIC PRESSURE OF 9.7 POUNDS PER SQUARE FOOT

By Clinton V. Eckstrom and John S. Preisser

Langley Research Center
Langley Station, Hampton, Va.

Technical Film Supplement L-1006 available on request.

NATIONAL AERONAUTICS AND SPACE ADMINISTRATION

For sale by the Clearinghouse for Federal Scientific and Technical Information
Springfield, Virginia 22151 – CFSTI price $3.00

FLIGHT TEST OF A 40-FOOT-NOMINAL-DIAMETER DISK-GAP-BAND PARACHUTE DEPLOYED AT A MACH NUMBER OF 2.72 AND A DYNAMIC PRESSURE OF 9.7 POUNDS PER SQUARE FOOT

By Clinton V. Eckstrom and John S. Preisser
Langley Research Center

SUMMARY

A 40-foot-nominal-diameter (12.2 meter) disk-gap-band parachute was flight tested as part of the NASA Supersonic Planetary Entry Decelerator (SPED-I) Program. The test parachute was deployed from an instrumented payload by means of a deployment mortar when the payload was at an altitude of 158 500 feet (48.2 kilometers), a Mach number of 2.72, and a free-stream dynamic pressure of 9.7 pounds per foot^2 (465 newtons per meter^2). Suspension line stretch occurred 0.46 second after mortar firing and the resulting snatch force loading was -8.1g. The maximum acceleration experienced by the payload due to parachute opening was -27.2g at 0.50 second after the snatch force peak for a total elapsed time from mortar firing of 0.96 second.

Canopy-shape variations occurred during the higher Mach number portion of the flight test ($M > 1.4$) and the payload was subjected to large amplitude oscillatory loads. A calculated average nominal axial-force coefficient ranged from about 0.25 immediately after the first canopy opening to about 0.50 as the canopy attained a steady inflated shape. One gore of the test parachute was damaged when the deployment bag with mortar lid passed through it from behind approximately 2 seconds after deployment was initiated. Although the canopy damage caused by the deployment bag penetration had no apparent effect on the functional capability of the test parachute, it may have affected parachute performance since the average effective drag coefficient of 0.48 was 9 percent less than that of a previously tested parachute of the same configuration.

INTRODUCTION

The NASA Planetary Entry Parachute Program (PEPP) was established to provide data on parachute performance in low density environments (ref. 1). The test conditions of interest were a combination of low supersonic velocities and low dynamic pressures to simulate some proposed planetary entry conditions. Because the results of the PEPP tests were favorable (refs. 2 to 9), the series was extended to provide test data at higher

supersonic velocities but at the same low dynamic pressure. This extension was called the Supersonic Planetary Entry Decelerator (SPED-I) Program.

This report presents results from the second test of a 40-foot-nominal-diameter (12.2 meter) disk-gap-band parachute in the SPED-I series. For the first test, an identical parachute had been deployed at a Mach number of 1.91 and results are reported in reference 10.

Based on the highly successful outcome of that test, it was decided to deploy an identical parachute at a Mach number of 2.7 and at a dynamic pressure of 10 pounds per foot^2 (479 newtons per meter^2). The primary objective of this test was to evaluate the deployment and operational capabilities of the test parachute with deployment initiated at a significantly higher Mach number than the test of reference 10.

Motion-picture film supplement L-1006 is available on loan; a request card and a description of the film are included at the back of this paper.

SYMBOLS

a_l linear acceleration along longitudinal axis of payload, g units

$C_{A,o}$ nominal axial-force coefficient, $-\frac{m_{total} g a_l}{q_\infty S_o}$

$\left(C_{D,o}\right)_{eff}$ effective nominal drag coefficient

D_o nominal diameter, $\left(\frac{4S_o}{\pi}\right)^{1/2}$, feet (meters)

g acceleration due to gravity, 32.2 feet/second^2 (9.81 meters/second^2)

M Mach number

m mass, slugs (kilograms)

q_∞ free-stream dynamic pressure, $\frac{1}{2}\rho_\infty V^2$, pounds per foot^2 (newtons per meter^2)

S_o nominal surface area of parachute canopy including gap and vent, feet^2 (meters^2)

S_p projected area of parachute canopy, feet^2 (meters^2)

t time from vehicle lift-off, seconds

t' time from mortar firing, seconds

V true airspeed, feet per second (meters per second)

W total weight of payload-parachute system

z_E distance along local vertical axis Z_E

ρ_∞ free-stream atmospheric density, slugs per foot^3 (kilograms per meter^3)

Dots over symbols denote differentiation with respect to time.

TEST SYSTEM

The payload was carried to the test point by an Honest John – Nike-Nike rocket system. A photograph of the rocket vehicle is presented as figure 1. The test payload, shown in figure 2, and the onboard instrumentation (tensiometer, three orthoganally mounted accelerometers, gyro platform, and two 16-mm cameras) have been described in reference 4. The total descent weight of the payload-parachute system was 282 pounds (128 kilograms). The suspended payload weight was 245 pounds (111 kilograms) including the attachment bridle and tensiometer.

TEST PARACHUTE

The test parachute was a disk-gap-band (DGB) design having a nominal diameter of 40 feet (12.2 meters). Figure 3 presents the dimensional details of a gore and the general parachute-payload configuration. The test parachute was fabricated from the same drawings and at the same time as the one described in detail in reference 10; therefore, only a brief description is presented in the following table:

Parachute type	Disk-gap-band
Nominal diameter, D_o	40 ft (12.2 m)
Nominal area, S_o	1256 ft^2 (116 m^2)
Number of gores and suspension lines	32
Geometric porosity	12.5 percent

Canopy cloth weight	2.0 oz/yd^2 (68 g/m^2)
Suspension line rated tensile strength	550 lb (2450 N)
Total parachute weight	37 lb (16.8 kg)
Weight of parachute canopy, lines, post-reefing system and upper riser	34 lb (15.4 kg)
Weight of swivel and intermediate riser	3 lb (1.4 kg)

RESULTS AND DISCUSSION

Test Data

The flight test vehicle was launched at 10:45 a.m. m.s.t. on October 17, 1967, at White Sands Missile Range, New Mexico. Figure 4 presents the flight sequence and the recorded times for significant flight events. Time histories of altitude and relative velocity for the first 360 seconds of the flight are shown in figure 5. For all tests in both the PEPP and SPED-I series, the payload was in the ascent portion of the flight trajectory at the time the parachute was deployed; for this flight, mortar firing occurred 66.82 seconds from launch.

In order to provide meteorological data for use in analysis of parachute test data, an Arcas meteorological sounding rocket was launched 1 hour and 15 minutes after the flight to measure upper altitude winds and temperatures. The rocket sounding information was supplemented by data from a rawinsonde which was released near the time the flight test vehicle was launched. Upper atmospheric winds as determined from the rocket sounding are presented in figure 6. Atmospheric density derived from both measured temperature profiles is presented in figure 7.

The measured atmospheric data were used with radar track and telemetered accelerometer data after initiation of deployment to determine time histories of payload true airspeed, Mach number (fig. 8), and dynamic pressure (fig. 9). By definition, the initiation of the deployment sequence corresponds to mortar firing ($t' = 0$ in the figs.). Parachute deployment was initiated at a true airspeed of 2865 feet per second (873 meters per second) or $M = 2.72$, a dynamic pressure of 9.7 pounds per foot^2 (465 newtons per meter^2), and an altitude of 158 500 feet (48.2 kilometers) above mean sea level. The altitude of the parachute-payload system during the first 23 seconds after parachute deployment, as determined by radar tracking, is presented in figure 10.

The tensiometer electrical lead was severed during ejection of the parachute from the mortar and, as a result, no record was obtained of the load transmitted through the riser line. However, the accelerations applied to the payload were measured by three mutually perpendicular accelerometers and these data are presented in figure 11. The peak acceleration of -6.6g at $t' = 0.18$ second resulted from the full length deployment

of the parachute attachment system. A larger load peak of -8.1g at $t' = 0.46$ second is a result of the snatch force associated with full length deployment of the parachute suspension lines. The maximum load associated with the opening of the parachute canopy was -27.2g at $t' = 0.96$ second. (Based on a payload weight of 245 pounds (111 kilograms), the maximum applied force was determined to be 6660 pounds (29 600 newtons).) Immediately after the peak opening load was recorded, the acceleration dropped to near zero (-0.5g) at $t' = 1.06$ seconds, and increased again to -18.6g at $t' = 1.59$ seconds. Thereafter, the acceleration history varied considerably from a ±8g variation at $t' = 2$ seconds decreasing to a ±4g variation at $t' = 5$ seconds. The large amplitude variations are believed to be associated with the suspension line elastic oscillations. The appendix to this report presents equations used in a simple mathematical model constructed to simulate the payload acceleration time history. A close agreement between the flight accelerations and simulated accelerations is obtained when the payload and parachute are assumed to be point masses connected by an elastic member (suspension lines).

As mentioned previously, the onboard instrumentation also included a miniature attitude reference system (gyro platform) and two cameras. Prior to launch, the gyro platform was subjected to an operational offset procedure (described in ref. 6) to compensate for expected high altitude wind effects. Shortly after the successful completion of the offset procedure, the gyro platform malfunctioned; therefore, no flight data were obtained. Good quality film was obtained from both cameras from the recovered payload.

Analysis of Parachute Performance

Deployment.- The test parachute was deployed from the payload at an average ejection velocity of 112 feet per second (34.1 meters per second) based on a total suspension line plus attachment system length of 51.5 feet (15.7 meters) and a measured time to line stretch of 0.46 second. As mentioned previously, the resulting snatch load was -8.1g.

Canopy inflation.- The canopy inflation process was somewhat erratic in that the canopy shape did not become steady until several seconds after deployment. Selected frames from the payload aft camera film showing initial canopy inflation, canopy collapse, canopy reinflation and shape variations, and the fully opened canopy are presented in figure 12.

The mortar-type deployment method used for these tests (described in ref. 4) uses the inertia of the packing bag and mortar lid (which are attached to form a single unit) to assure that the deployment bag strips off the canopy completely. Photographic evidence indicates that the deployment bag and mortar lid, which had a combined weight of 3.75 pounds (1.7 kilograms), stripped from the canopy properly. On previous PEPP

rocket-launched flight tests, the trajectories of the parachute and deployment bag with mortar lid after bag strip were sufficiently different to avoid collision after canopy inflation. However, on this flight test, there was essentially no difference in the flight paths of the parachute-payload system and the deployment bag and lid. Because of the higher deceleration rate of the payload-parachute system relative to that of the bag and lid, the deployment bag and mortar lid collided with and penetrated the parachute canopy from behind. This penetration occurred approximately 2 seconds after the deployment mortar fired. As a result, one gore of the canopy was damaged extensively. The deployment bag can be seen entangled in the band portion of canopy in figure 12(c), at $t' = 2.17$ seconds, soon after it penetrated the canopy. The hole in the canopy can also be seen in that figure. Visible in figure 12(c), at $t' = 2.30$ seconds, is a piece of canopy cloth which ripped away from the canopy as a result of the damage. (Similar bag penetrations occurred in the PEPP balloon-launched tests reported in refs. 3, 8, and 9.) Figure 13 presents the ratio of the parachute projected area S_p to the projected area attained by the fully opened parachute during descent $S_{p,final}$ for the first 9 seconds after deployment. Also shown in figure 13 is the time of deployment bag penetration. As seen from figures 12 and 13, the canopy inflated rapidly to the full open condition at $t' = 0.95$ second. The Mach number was 2.62 at this time. However, the projected area decreased immediately and then increased again on an irregular basis (due to shape variations in both the band and disk portion of the canopy) until $t' = 7$ seconds. After $t' = 7$ seconds, the disk portion of the canopy remained fully inflated and canopy projected area variations were primarily due to slight variations in the shape of the band portion of the canopy as can be seen in figure 12(c). At the time a stable inflation was achieved, the Mach number was 1.4. On the previous test of an identical parachute (ref. 10), the deployment was at a lower Mach number; however, stable inflation was also achieved at a Mach number of approximately 1.4, which occurred 1.6 seconds after deployment.

A detailed analysis of the cause or causes of the shape variation is outside the scope of this report. The effect of the suspension line oscillations in hindering the stabilization of canopy shape is not known. No analysis has been performed to determine what effects the rapidly changing mass flow and fluctuating canopy shock wave position may have had on the inability of the canopy to stabilize its shape during the high Mach number portion of the flight.

Drag efficiency.- The variation of the computed nominal axial-force coefficient $C_{A,o}$ as determined from the accelerometer data in 0.005-second increments, is presented in figure 14 as a function of time from parachute deployment. In addition to the time scale, a Mach number scale is shown for reference. The axial-force coefficient was determined by the following equation:

$$C_{A,o} = -\frac{m_{total} g a_l}{q_\infty S_o}$$

The large variations in $C_{A,o}$, which are present when the calculation is performed in 0.005-second time increments, directly reflect the large variations found in the longitudinal accelerometer time history of figure 11. As indicated by the simulation contained in the appendix, sudden changes in parachute drag-producing area can force the elastic suspension line system to oscillate. The longitudinal accelerometer will record the effects of this oscillatory load as transmitted to the payload. However, if the $C_{A,o}$ calculation is based on 0.2-second averages of the accelerometer data (also shown in fig. 14), the higher frequency variations are averaged throughout the time increment and a representation of the drag efficiency of the parachute is obtained.

Note that the average $C_{A,o}$ is increasing (from about 0.25 to 0.50) with time somewhat proportional to the increase in parachute frontal area that was shown previously in figure 13. Although initially this average coefficient was lower than that measured for the first 3 or 4 seconds from mortar firing during the test of the identical parachute reported in reference 10, the system was decelerated rapidly as desired, and good drag efficiency was exhibited during the remainder of the flight. The estimated uncertainty in this average $C_{A,o}$, based on a first-order error analysis using a 3-percent density error, 3-percent velocity error, and 0.5-g accelerometer uncertainty, varied from ±0.03 at 1.0 second to ±0.08 at 6.0 seconds.

Figure 15 presents the variation of the vertical descent velocity and the effective nominal drag coefficient with altitude. The values of effective drag coefficient are based on vertical descent velocity and acceleration and the system weight as shown by the following equation:

$$\left(C_{D,o}\right)_{eff} = \frac{2m_{total}}{\rho_\infty \dot{z}_E^2 S_o}\left(g - \ddot{z}_E\right)$$

During the descent portion of the flight test, the average effective nominal drag coefficient $\left(C_{D,o}\right)_{eff}$ was about 0.48. The small variations from this average value are within the uncertainty in $\left(C_{D,o}\right)_{eff}$ which was estimated to be ±0.04, with a 3-percent density error, 3-percent velocity error, and 10-percent acceleration error. Although individual data points may have an uncertainty of ±0.04 the average of all the data points over the entire altitude interval is a good indication of the performance of the parachute. For this flight test the average value of the effective drag coefficient was about 9 percent less than that of an identical parachute tested previously as reported in reference 10. The only known difference in the conditions between this flight and the previous one was

the hole in the disk portion of the canopy caused by the penetration of the deployment bag. The hole size was approximately 1 percent of the projected area.

Stability.- As mentioned previously, no gyro platform data were available for an analysis of the stability of the payload-parachute system during the deceleration and descent portion of the test period. However, stability data from the earlier test of an identical test parachute have been presented in reference 10. The nose camera film obtained during the presently reported flight test indicates that payload pitch-yaw motions averaged higher than those reported in reference 10 during the descent period when the system was above 100 000 feet (30.5 km). These large motions might be expected in view of the unsymmetric canopy open area caused by the penetration of the deployment bag.

Analysis of recovered parachute.- As mentioned previously, one gore of the test parachute was damaged by penetration of the deployment bag. A sketch of the damaged area, which was in gore 8, is shown in figure 16. A large piece of cloth was torn out of the midpanel of the gore, as seen in figure 12(c), at $t' = 2.30$ seconds, but the tears did not propagate past the diagonal panel seams above and below the damaged panel. The deployment bag with mortar lid caused slight additional damage to the band at gore 10 where the material was torn for approximately 5 inches (12.7 centimeters) near the lower edge of the band. Marks on the canopy at this point, as well as the shape of the tear indicated that the deployment bag and mortar lid caused this tear.

The band portion of the canopy was slightly damaged in two additional places. One of these was a 3-inch (7.6 centimeter) tear along the reinforcement tape on the upper edge of the band on gore 1. The second was a separation of the fill threads for approximately 4 inches (10 centimeters) along the upper edge of the band on gore 25. The warp threads were not broken in this area. The cause of this damage has not been specifically identified but it may have been caused by fluttering of the panel during the higher Mach number portion of the flight.

Nearly all parachute suspension lines and post-reefing lines had discolorations and evidence of abrasion. (Although the post-reefing system was not used on this flight test, the parachute was equipped with the necessary lines and rigging in the canopy. A description of a similar post-reefing system may be found in ref. 5.) This abrasion damage may have resulted from friction, since an examination of the aft camera film revealed that the suspension lines experienced whipping almost constantly during the initial portion of the test.

After the recovered parachute had been examined for damage, several measurements were taken to determine if any dimensional changes had resulted from the preflight sterilization heat cycle. It was found that all canopy structural members – that is, radial tapes, skirt tape, gap edge tapes, and vent edge tapes – had shrunk about 8 percent

in length. Although the canopy cloth had not shrunk, the nominal area, as defined by the gore edge tapes, was reduced to 1065 feet^2 (99 meters^2) which is a reduction of 15 percent from the original area. This gives a revised nominal diameter of 36.8 feet (11.2 meters). The shrinkage of the identical canopy tested previously (ref. 10) was also found to be the same. The length of suspension lines on the parachutes had not changed. Because the canopy cloth did not shrink and the gore edge reinforcement tapes did, the result was a canopy of reduced size with excessive material fullness. Since the effect of this change is unknown the original constructed nominal area S_o = 1256 feet^2 (116 meters^2) was used as the reference area for data analysis purposes.

CONCLUSIONS

A 40-foot-nominal-diameter (12.2 meter) disk-gap-band parachute was deployed from an instrumented payload by means of a deployment mortar when the payload was at an altitude of 158 500 feet (48.2 kilometers), a Mach number of 2.72, and a free-stream dynamic pressure of 9.7 pounds per foot^2 (465 newtons per meter^2). Based on an analysis of the data, the following conclusions are made:

1. The mortar properly ejected the parachute system from the payload.

2. The parachute canopy inflation process began immediately and was successfully completed after several cyclic variations of canopy shape and frontal area.

3. The large amplitude variations recorded by the payload accelerometer are believed to be principally a result of an oscillation set up in the parachute elastic suspension line system.

4. An average axial-force coefficient exhibited during the high deceleration portion of the test varied from about 0.25 immediately after deployment (when the canopy shape variations were greatest) to about 0.50 at 7 seconds after deployment when the canopy shape had stabilized to the full-inflated condition; effective drag coefficient during descent was 0.48.

5. The only significant damage sustained by the parachute canopy during the flight test was caused by the impact of the deployment bag with mortar lid overtaking the rapidly decelerating parachute-payload system. Damage caused by the parachute deployment bag and ejection mortar lid passing through the canopy apparently had little effect on the functional capability of the test parachute; however, the effective drag coefficient was 9 percent less and payload oscillations appeared greater than those for a previous test of an identical parachute where the canopy was undamaged.

6. Further study is needed to determine the effects of the sterilization heat cycle on the various properties of dacron parachute materials, particularly with regard to shrinkage and abrasion.

Langley Research Center,
National Aeronautics and Space Administration,
Langley Station, Hampton, Va., June 24, 1968,
709-10-00-01-23.

APPENDIX

ONE-DIMENSIONAL COUPLED OSCILLATOR SIMULATION

A simple mathematical model was constructed in order to analyze the response of the payload to the parachute drag force developed during canopy inflation and through the high deceleration portion of the test. The model is based on the assumption that the payload-parachute system can be described as point masses joined by elastic parachute suspension lines which act like a spring when a load is applied to them.

Consider two masses, m_1 (parachute) and m_2 (payload), coupled together by a spring (suspension lines) of stiffness k. The system is initially traveling to the right at an initial velocity V_o as shown in the following sketch, when a time-varying forcing function (parachute drag) is applied to m_1 in the opposite direction of the system motion (drag of the payload is assumed negligible).

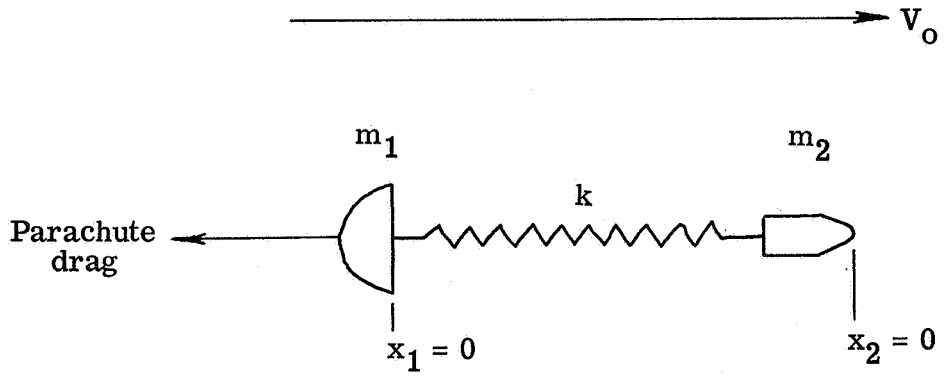

The one-dimensional equations of motion for the two masses are as follows: When $x_2 > x_1$; that is, when the spring is stretched,

$$m_1\ddot{x}_1 = -C_{A,o}S_o\left[\frac{S_p}{S_{p,final}}(t')\right]\left[\frac{1}{2}\rho_\infty(t')\dot{x}_1^2\right] + k(x_2 - x_1) - m_1 g \sin\theta \qquad (1a)$$

and

$$m_2\ddot{x}_2 = -k(x_2 - x_1) - m_2 g \sin\theta \qquad (1b)$$

where $\frac{S_p}{S_{p,final}}(t')$ is the time history of the normalized parachute canopy projected area (as shown in fig. 13), $\rho_\infty(t')$ is the atmospheric density environment experienced

(as can be obtained from figs. 7 and 10), and the values for the constants used in the simulation are

V_o = 2865 ft/sec (873 m/sec)

$m_1 g$ = 33 lb (147 N)

$m_2 g$ = 249 lb (1108 N)

$C_{A,o}$ = 0.48

S_o = 1256 ft^2 (116 m^2)

k = 2000 lb/ft (29 kN/m) (average value of stiffness for all 32 suspension lines acting together as an aggregate)

g sin θ = 29.4 ft/sec^2 (8.96 m/sec^2) (average component of acceleration due to gravity which acts along the longitudinal axis of the system)

A constraint was added to equations (1a) and (1b), so that when $x_2 < x_1$, there is no spring restoring force. This constraint allows the suspension lines to go slack rather than compressing, as a spring would; that is, when $x_2 < x_1$, the $k(x_2 - x_1)$ term will not appear in equation (1a) or (1b).

The two equations were programed on a digital computer and time histories of x_1, $\dot{x}_1$, $\ddot{x}_1$, x_2, $\dot{x}_2$, and $\ddot{x}_2$ were generated using a standard Runge-Kutta method. The initial conditions (t' = 0) were selected to be

$$x_1 = x_2 = 0$$

$$\dot{x}_1 = \dot{x}_2 = V_o$$

$$\ddot{x}_1 = \ddot{x}_2 = 0$$

APPENDIX

The simulated payload acceleration $\ddot{x}_2$ is shown in figure 17. A reasonable comparison is obtained between the time history of $\ddot{x}_2$ and the longitudinal component of payload acceleration (fig. 11) experienced during the flight. Peak accelerations are comparable and the frequency nature of both histories are similar. No external damping (aerodynamic or viscous) was included in the simulation. However, it is interesting to note that the parachute canopy provides its own damping through the $\frac{1}{2}\rho_\infty(t')\dot{x}_1^2$ term; the result of this is evident in figure 17. Conversely, for future tests of a similar nature where it is intended to deploy the test parachute at higher altitudes, it may be expected that less self-damping will result because the atmospheric density ρ_∞ will be correspondingly smaller.

REFERENCES

1. McFall, John C., Jr.; and Murrow, Harold N.: Parachute Testing at Altitudes Between 30 and 90 Kilometers. AIAA Aerodynamic Deceleration Systems Conference, Sept. 1966, pp. 116-121.

2. Eckstrom, Clinton V.; and Preisser, John S.: Flight Test of a 30-Foot-Nominal-Diameter Disk-Gap-Band Parachute Deployed at a Mach Number of 1.56 and a Dynamic Pressure of 11.4 Pounds Per Square Foot. NASA TM X-1451, 1967.

3. Bendura, Richard J.; Huckins, Earle K, III; and Coltrane, Lucille C.: Performance of a 19.7-Meter-Diameter Disk-Gap-Band Parachute in a Simulated Martian Environment. NASA TM X-1499, 1968.

4. Preisser, John S.; Eckstrom, Clinton V.; and Murrow, Harold N.: Flight Test of a 31.2-Foot-Diameter Modified Ringsail Parachute Deployed at a Mach Number of 1.39 and a Dynamic Pressure of 11.0 Pounds Per Square Foot. NASA TM X-1414, 1967.

5. Eckstrom, Clinton V.; Murrow, Harold N.; and Preisser, John S.: Flight Test of a 40-Foot-Nominal-Diameter Modified Ringsail Parachute Deployed at a Mach Number of 1.64 and a Dynamic Pressure of 9.1 Pounds Per Square Foot. NASA TM X-1484, 1967.

6. Preisser, John S.; and Eckstrom, Clinton V.: Flight Test of a 30-Foot-Nominal-Diameter Cross Parachute Deployed at a Mach Number of 1.57 and a Dynamic Pressure of 9.7 Pounds Per Square Foot. NASA TM X-1542, 1968.

7. Whitlock, Charles H.; Bendura, Richard J.; and Coltrane, Lucille C.: Performance of a 26-Meter-Diameter Ringsail Parachute in a Simulated Martian Environment. NASA TM X-1356, 1967.

8. Whitlock, Charles H.; Henning, Allen B.; and Coltrane, Lucille C.: Performance of a 16.6-Meter-Diameter Modified Ringsail Parachute in a Simulated Martian Environment. NASA TM X-1500, 1968.

9. Lundstrom, Reginald R.; Darnell, Wayne L.; and Coltrane, Lucille C.: Performance of a 16.6-Meter-Diameter Cross Parachute in a Simulated Martian Environment. NASA TM X-1543, 1968.

10. Preisser, John S.; and Eckstrom, Clinton V.: Flight Test of a 40-Foot-Nominal-Diameter Disk-Gap-Band Parachute Deployed at a Mach Number of 1.91 and a Dynamic Pressure of 11.6 Pounds Per Square Foot. NASA TM X-1575, 1968.

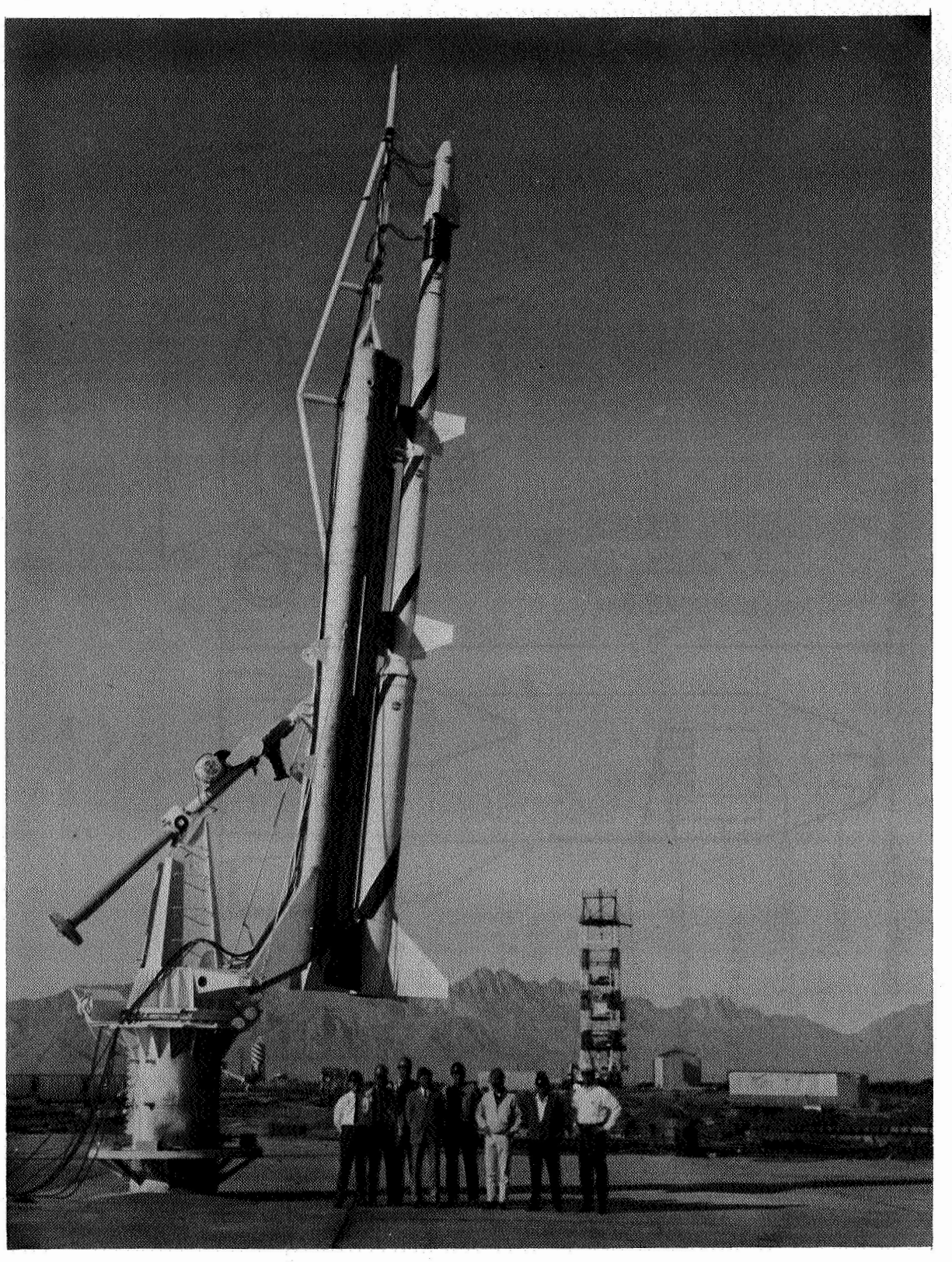

Figure 1.- Vehicle configuration. U.S. Army photograph. L-68-5626

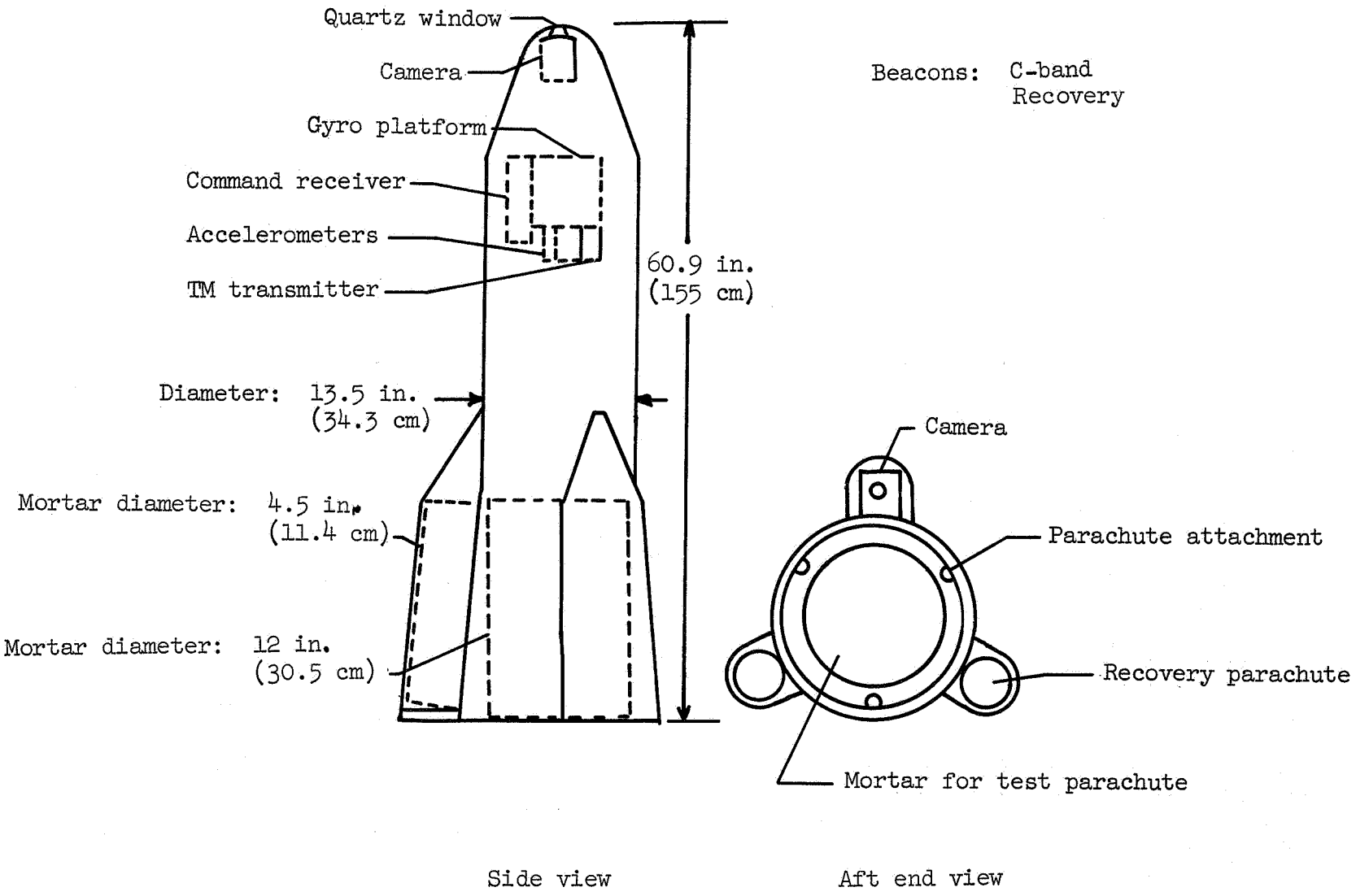

Figure 2.- Test payload.

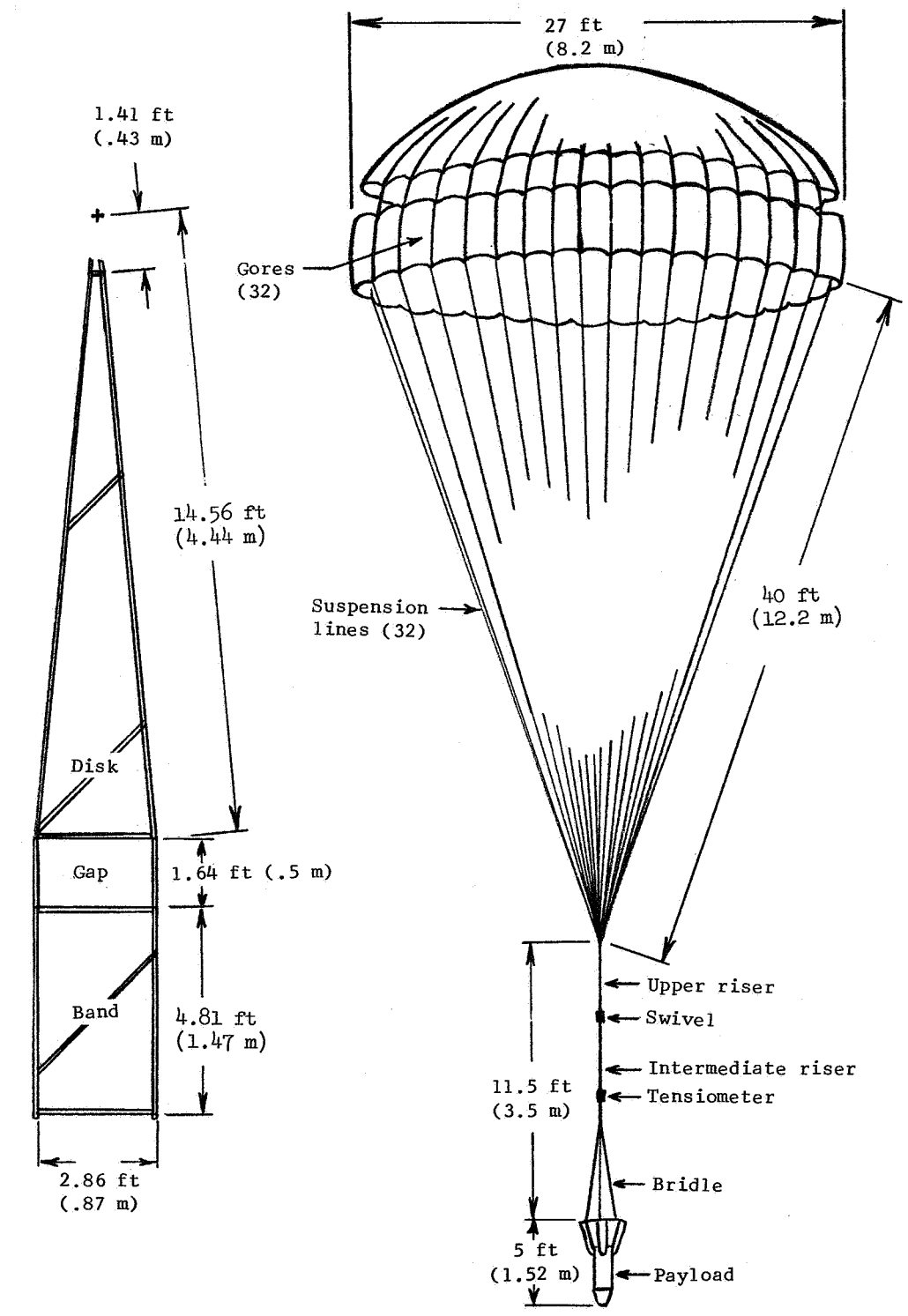

Figure 3.- Parachute gore dimensional details and flight configuration.

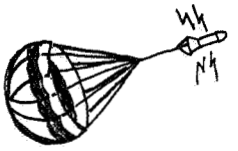

7. Maximum opening load

6. Mortar ejection of parachute

5. Radio command

4. Payload separation

3. Third-stage ignition

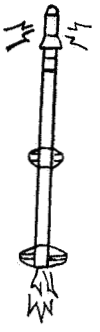

2. Second-stage ignition

Event	Time, t, sec
1	0
2	10.20
3	34.06
4	47.23
5	66.14
6	66.82
7	67.78
8	2466.0

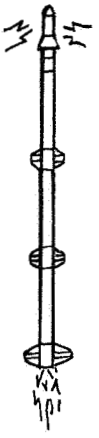

1. Vehicle lift-off.

8. Impact

Figure 4.- Flight sequence of events.

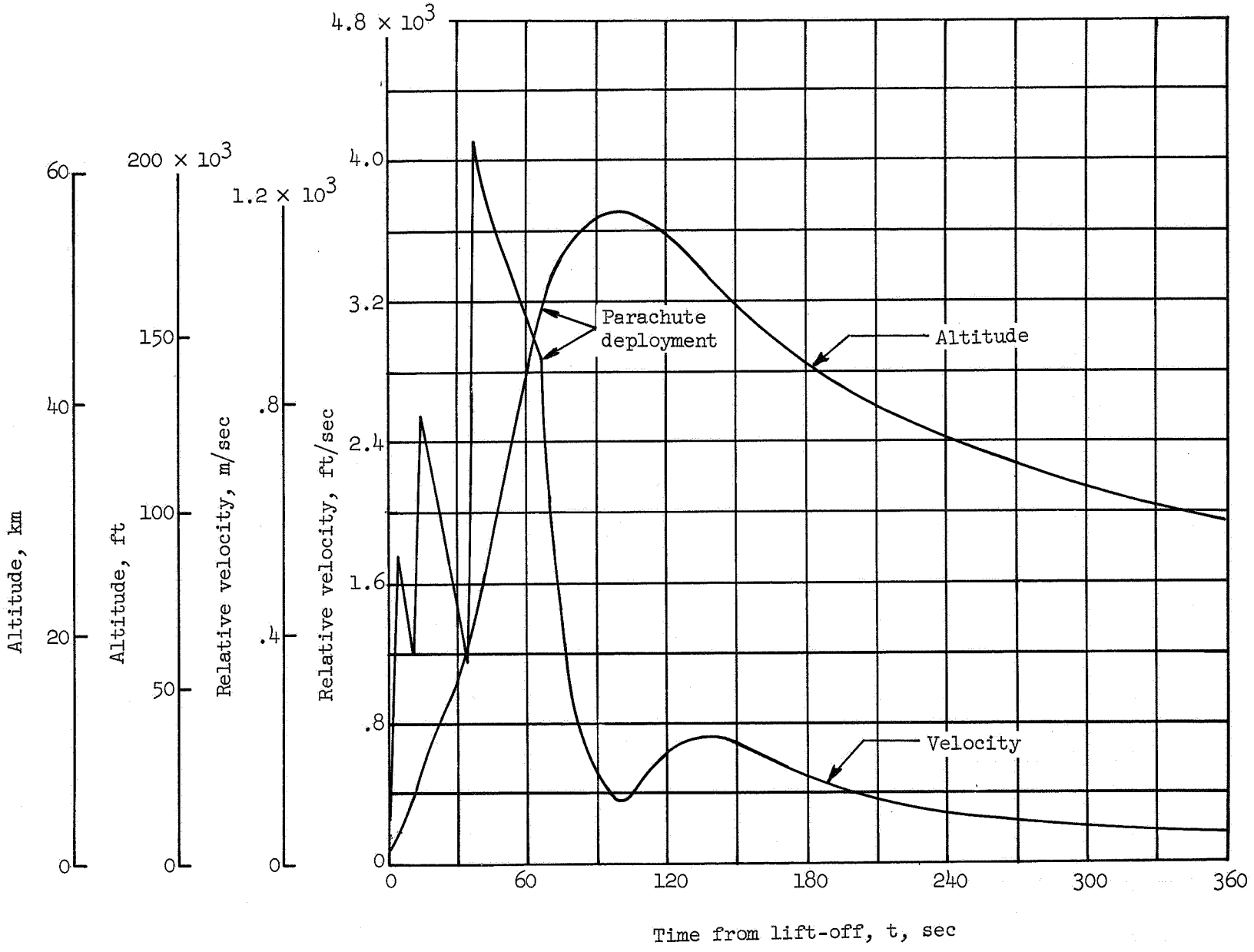

Figure 5.- Time histories of altitude and relative velocity.

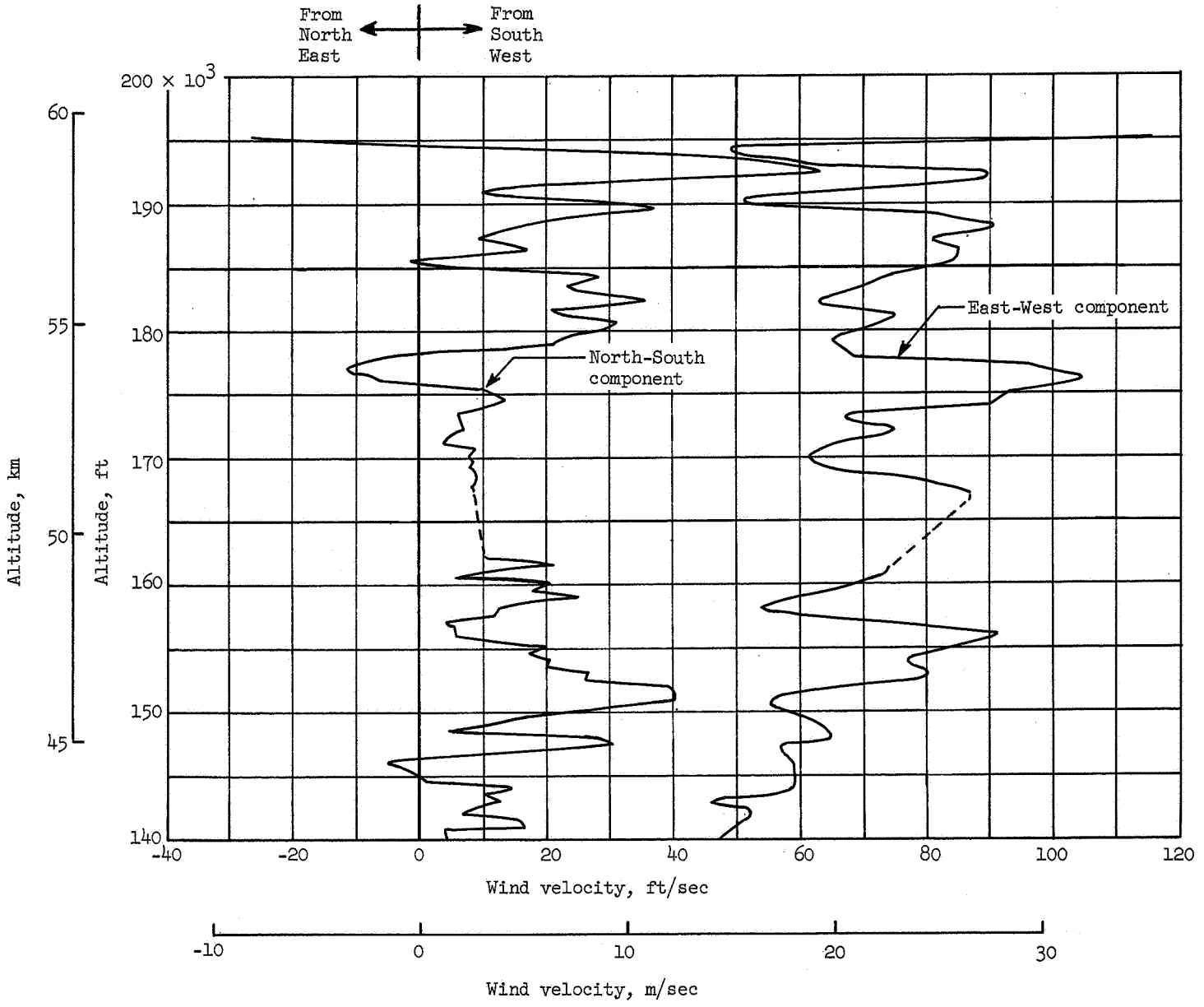

Figure 6.- Wind velocity profile in north-south and east-west components.

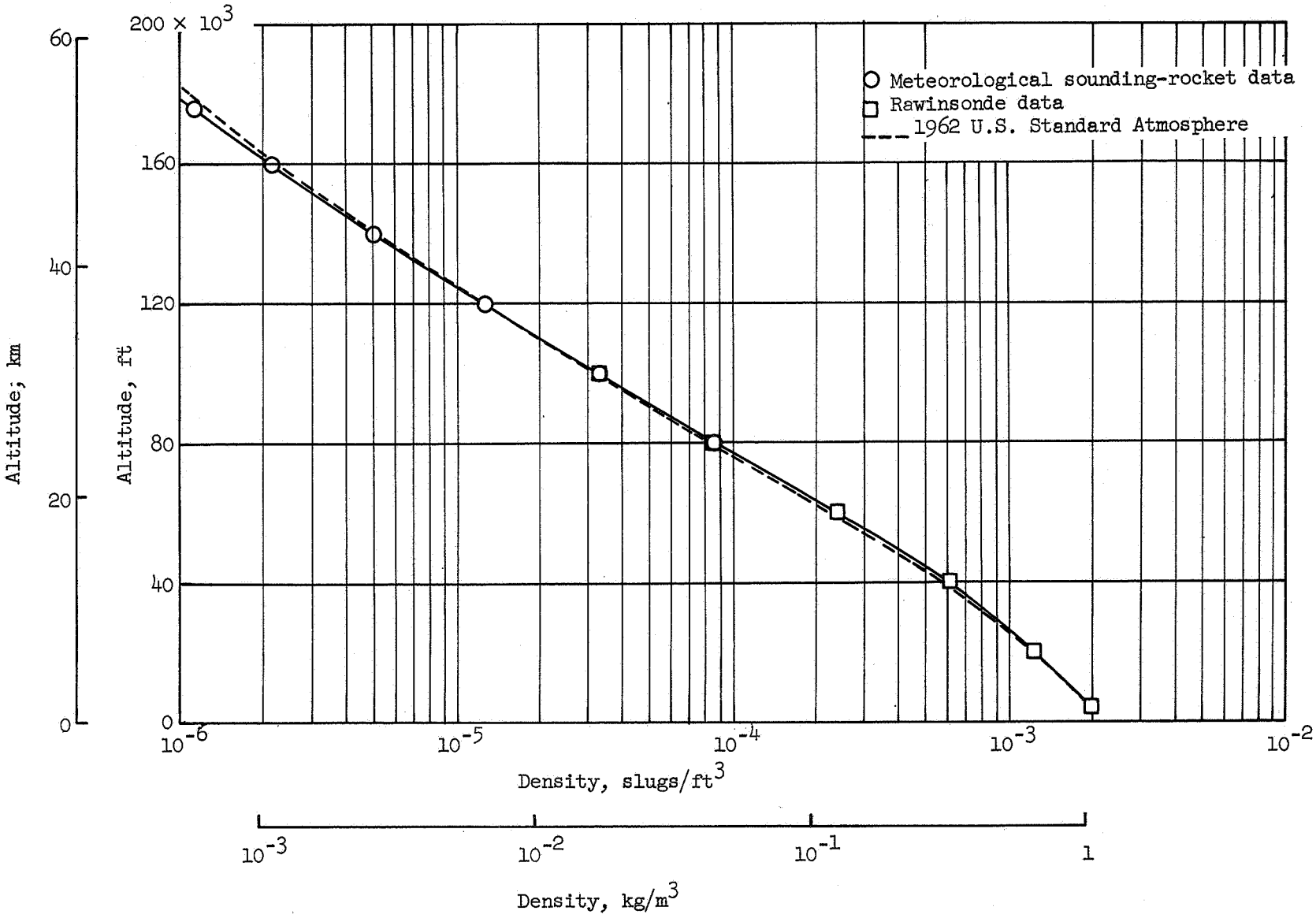

Figure 7.- Atmospheric density profile.

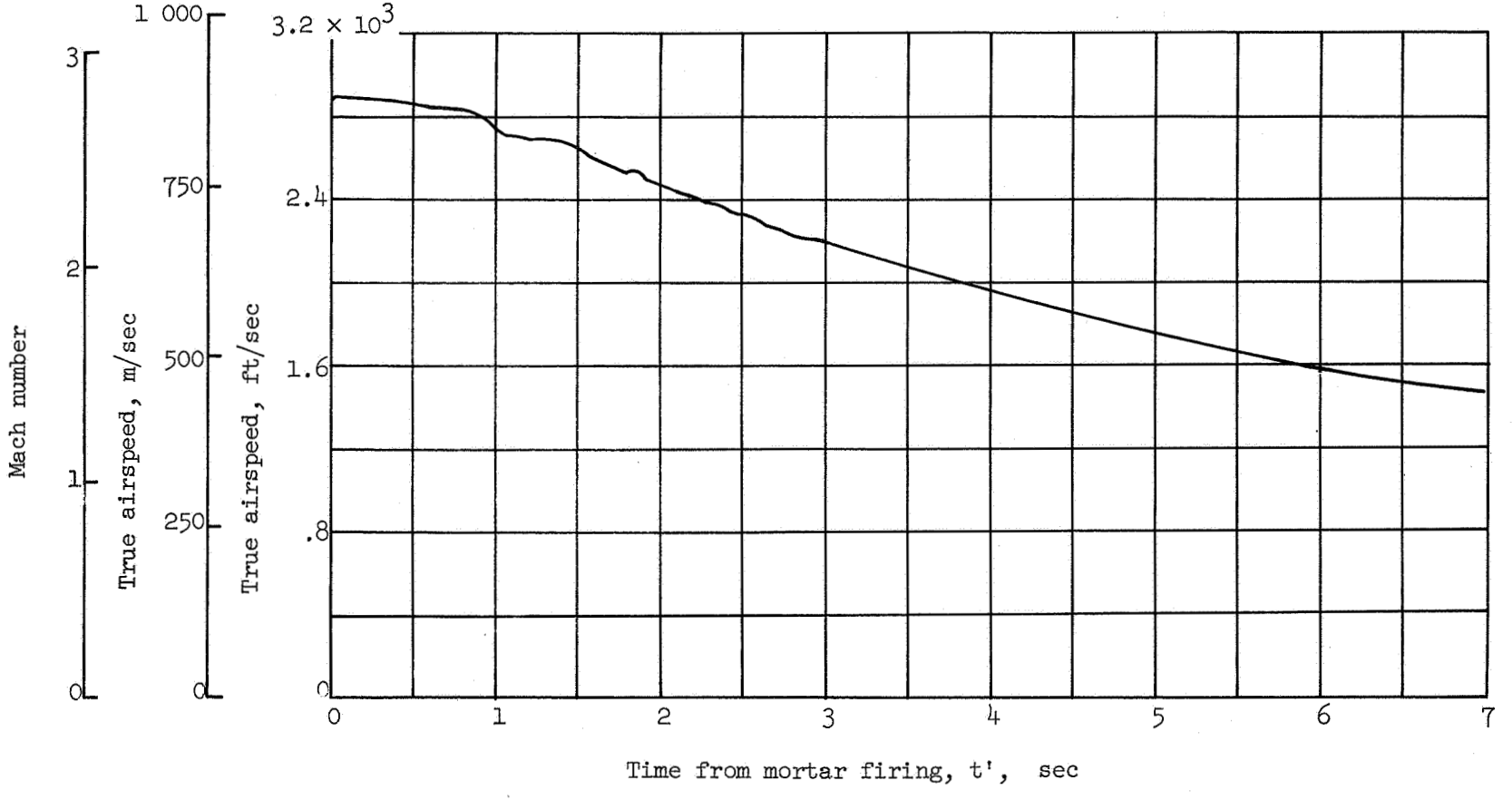

Figure 8.- Mach number and true airspeed time histories after mortar firing. Payload-parachute system velocity became subsonic at t' = 11.0 seconds.

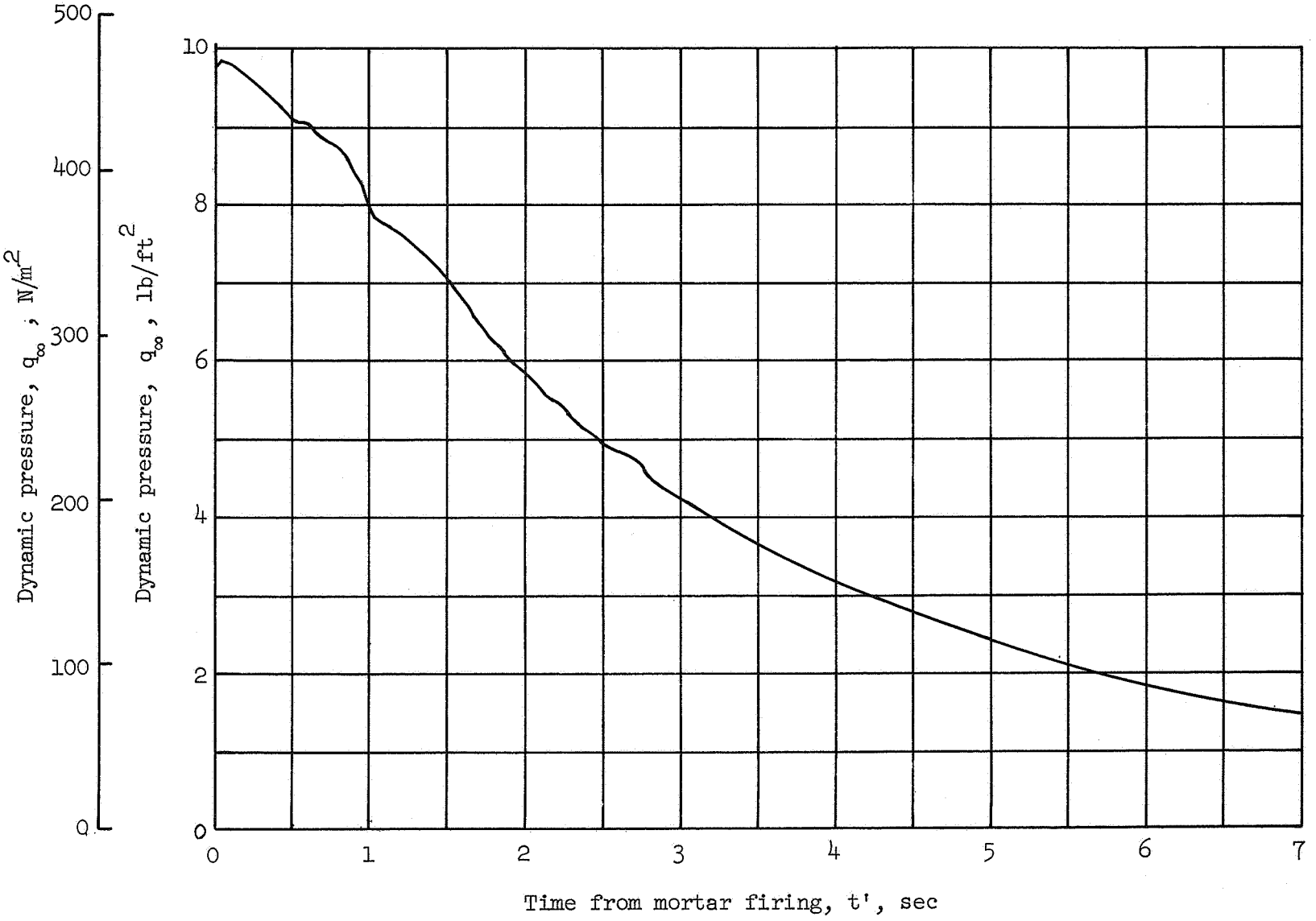

Figure 9.- Dynamic-pressure time history after mortar firing. For steady-state equilibrium descent, $q_\infty = \frac{W}{(C_{D,o})_{eff} S_o} = 0.47$ lb/ft^2 (22.5 N/m^2).

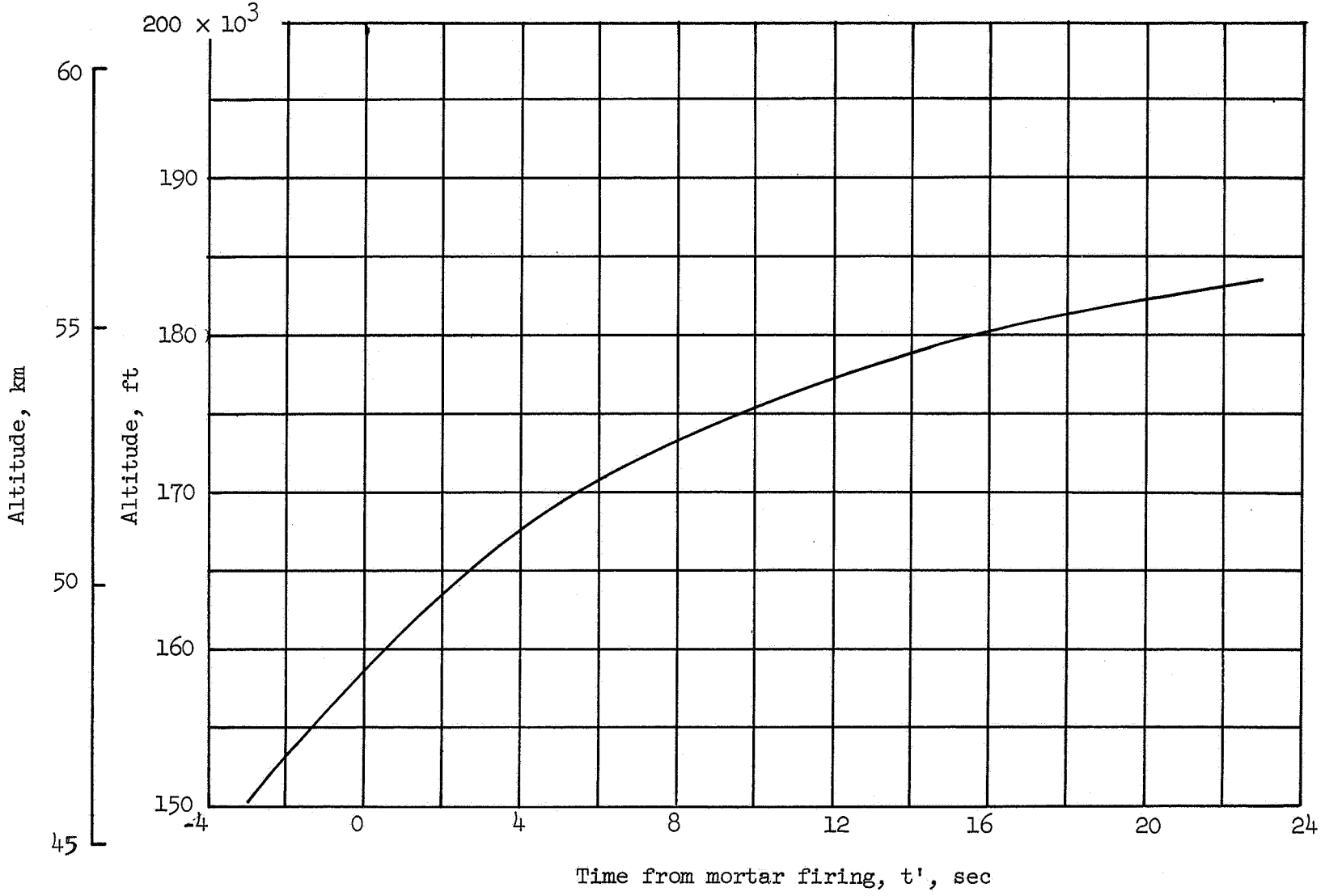

Figure 10.- Altitude time history for the first 23 seconds after mortar firing.

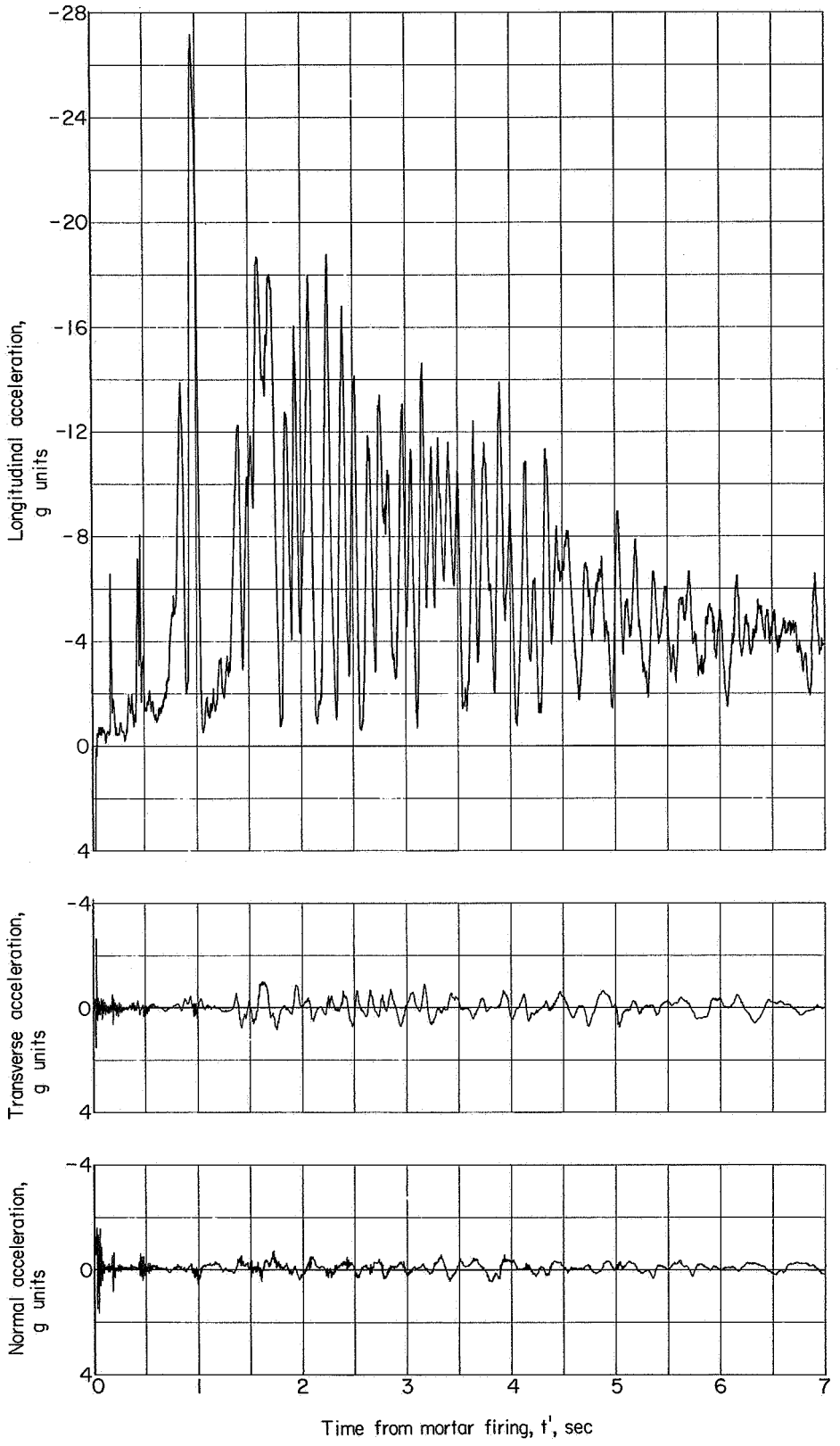

Figure 11.- Acceleration time histories.

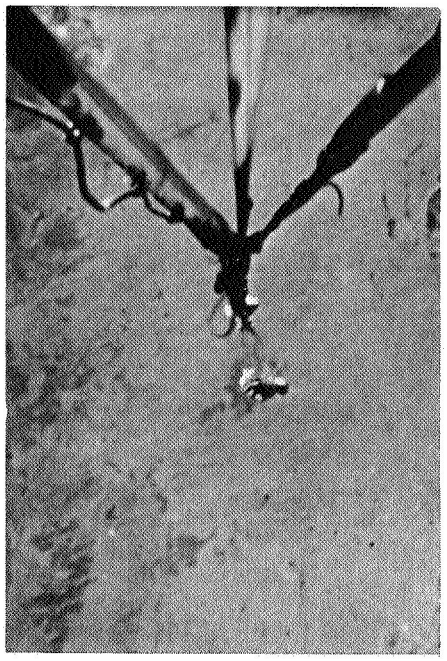

t' = .45 second

t' = .65 second

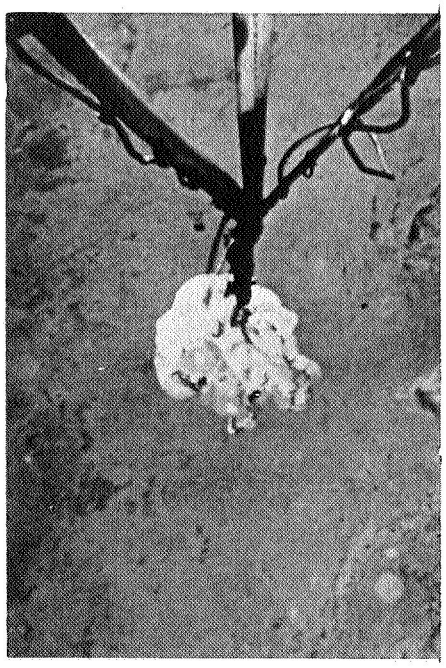

t' = .70 second

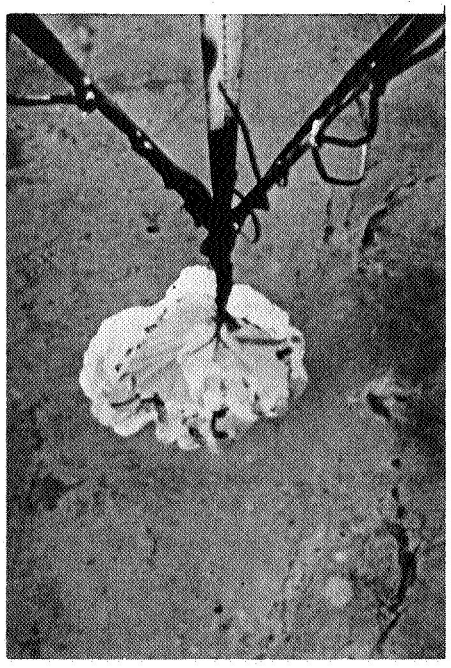

t' = .75 second

(a) Initial canopy inflation sequence. L-68-5627

Figure 12.- Onboard camera photographs.

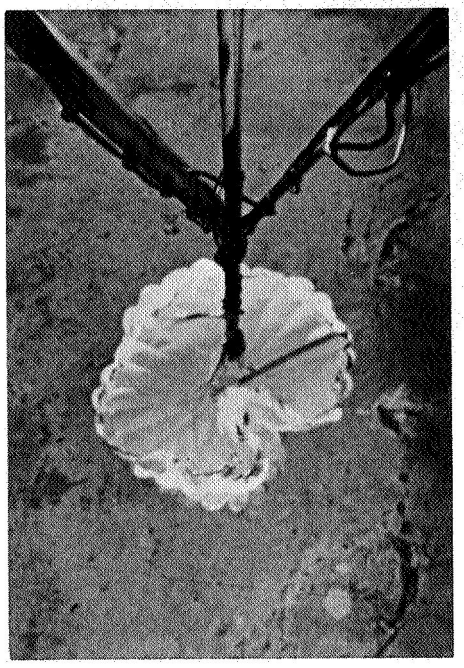

t' = .82 second

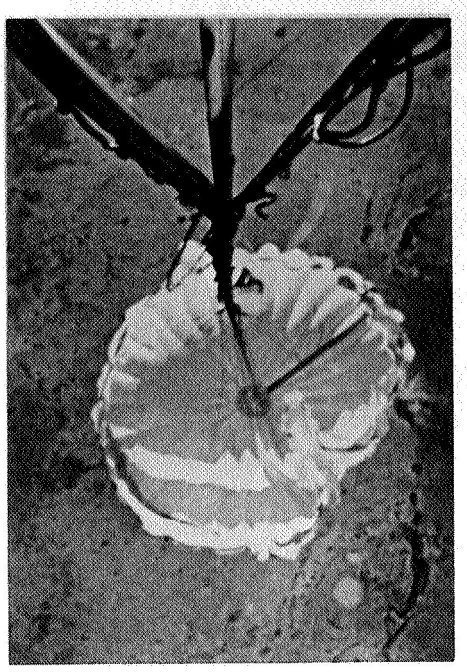

t' = .87 second

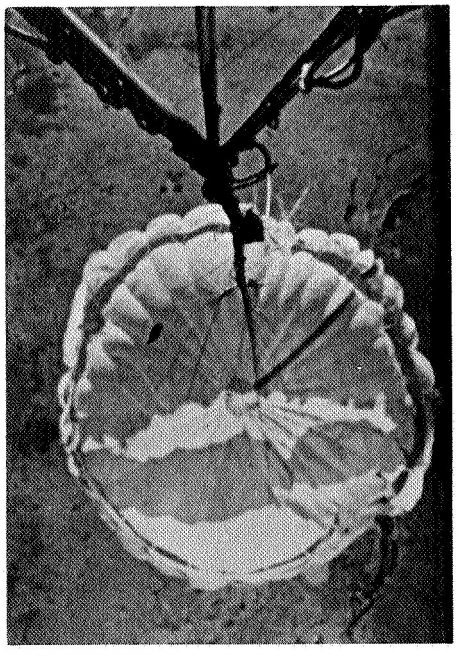

t' = .92 second

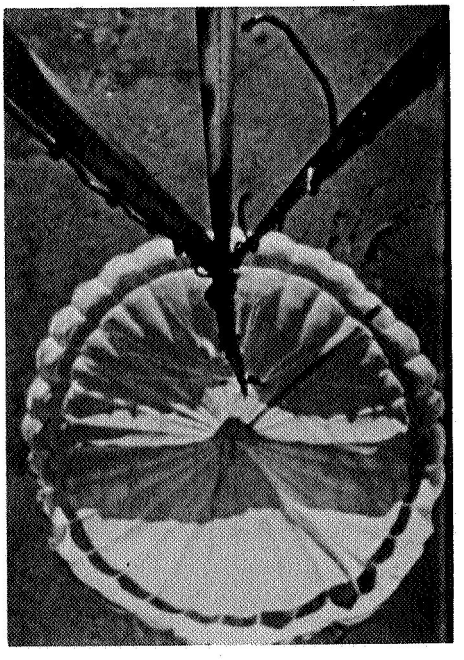

t' = .95 second

(a) Concluded.

L-68-5628

Figure 12.- Continued.

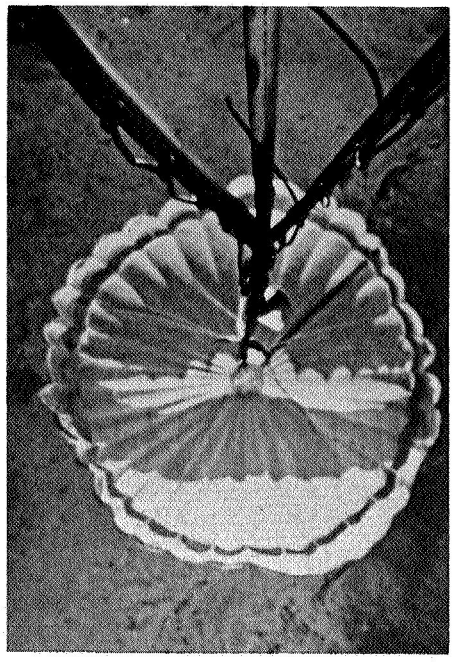

t' = .97 second

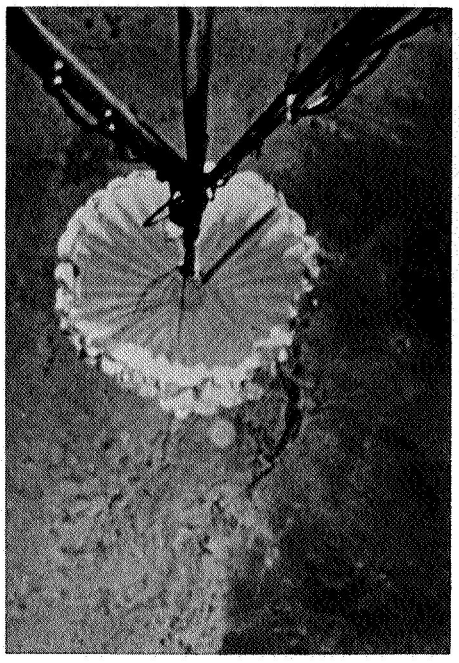

t' = 1.02 seconds

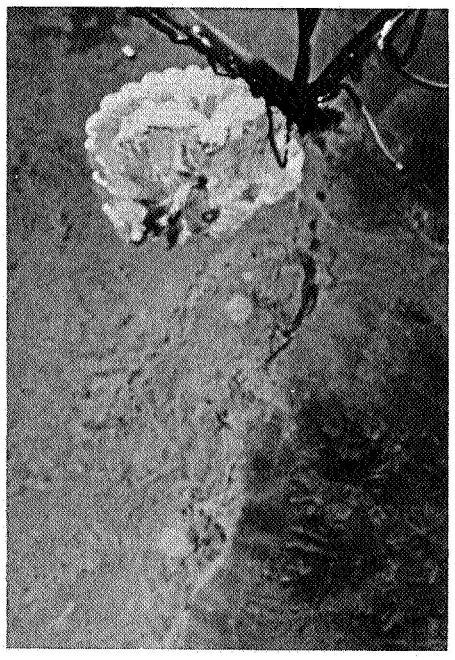

t' = 1.07 seconds

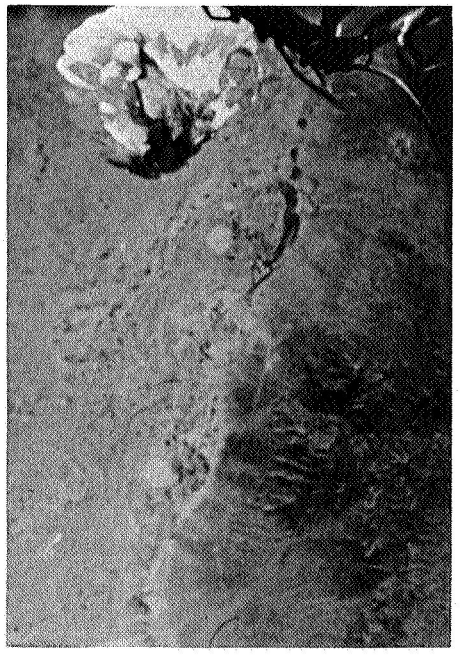

t' = 1.10 seconds

(b) Canopy collapse sequence. L-68-5629

Figure 12.- Continued.

t' = 1.40 seconds

t' = 1.45 seconds

t' = 1.50 seconds

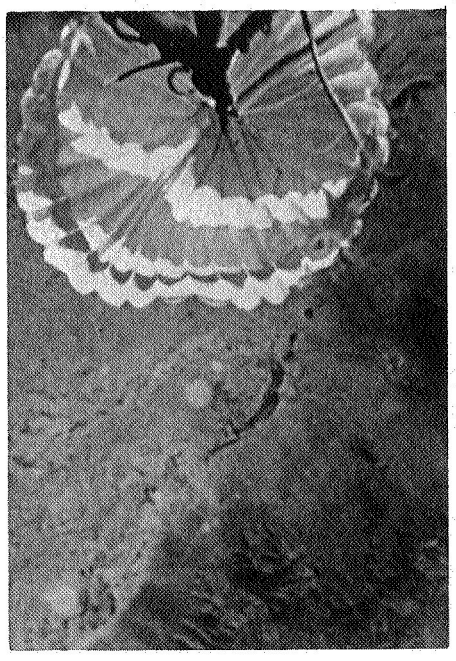

t'= 1.63 seconds

(c) Canopy reinflation sequence. L-68-5630

Figure 12.- Continued.

t' = 1.83 seconds

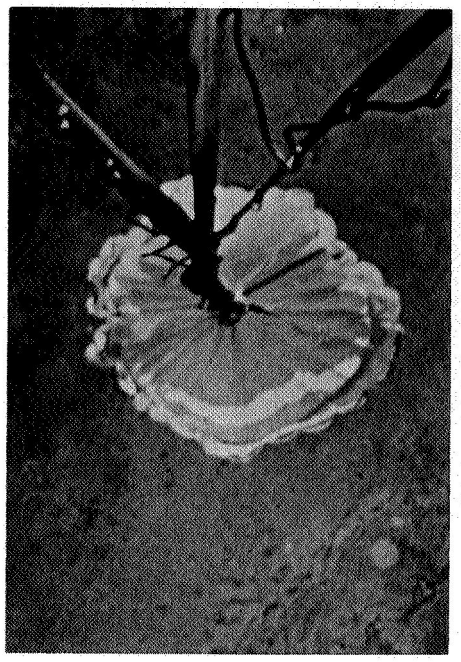

t' = 1.90 seconds

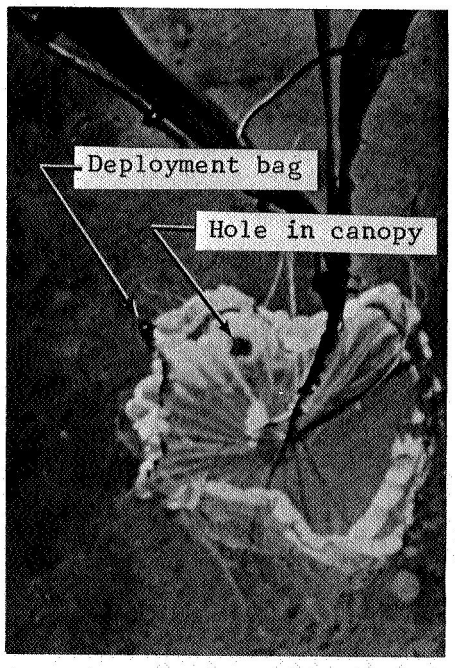

t' = 2.17 seconds

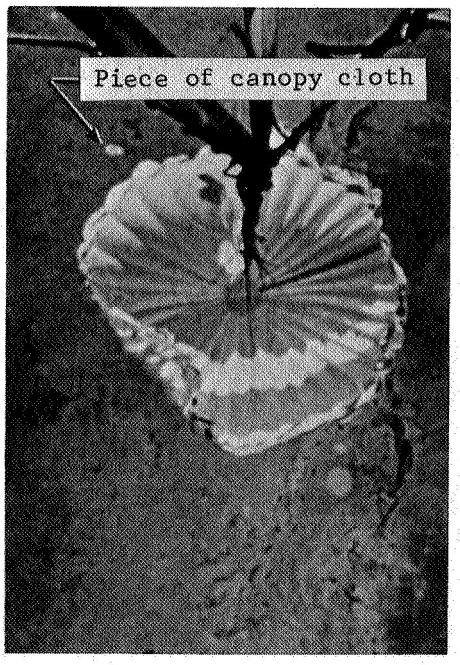

t' = 2.30 seconds

(c) Continued.

L-68-5631

Figure 12.- Continued.

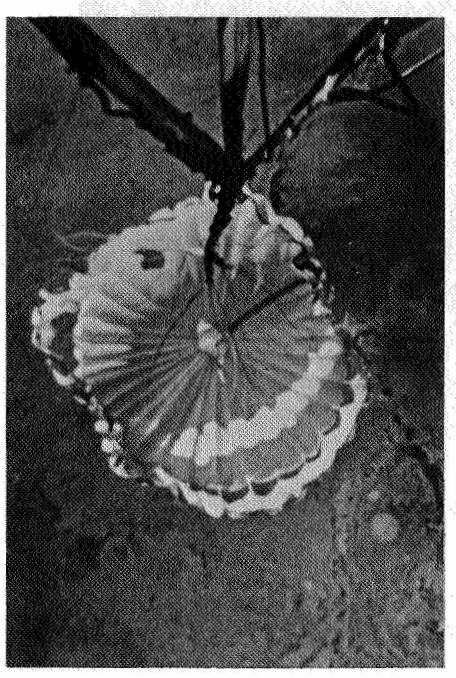

t' = 2.55 seconds

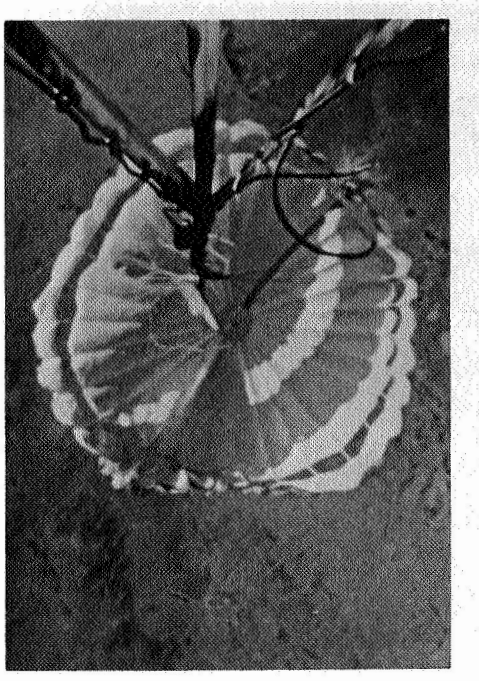

t' = 2.80 seconds

t' = 2.93 seconds

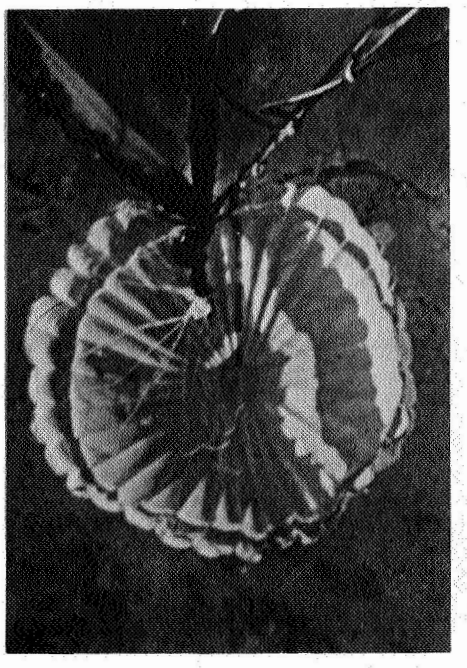

t' = 3.22 seconds

(c) Continued.

L-68-5632

Figure 12.- Continued.

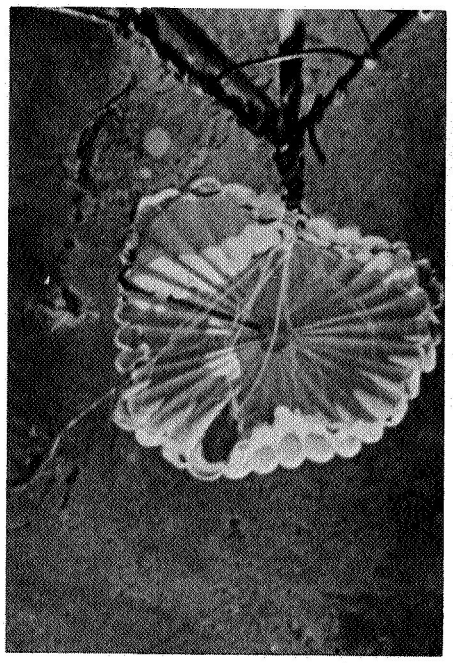

t' = 4.14 seconds

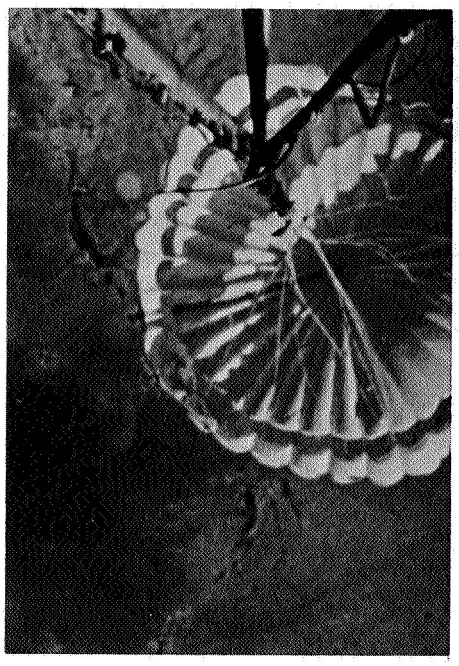

t' = 4.70 seconds

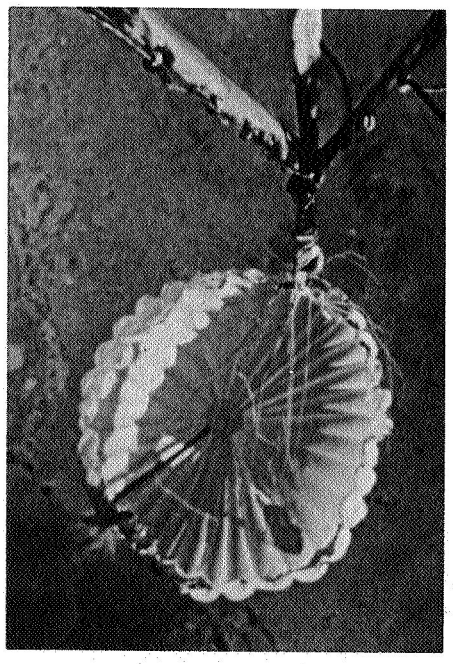

t' = 4.67 seconds

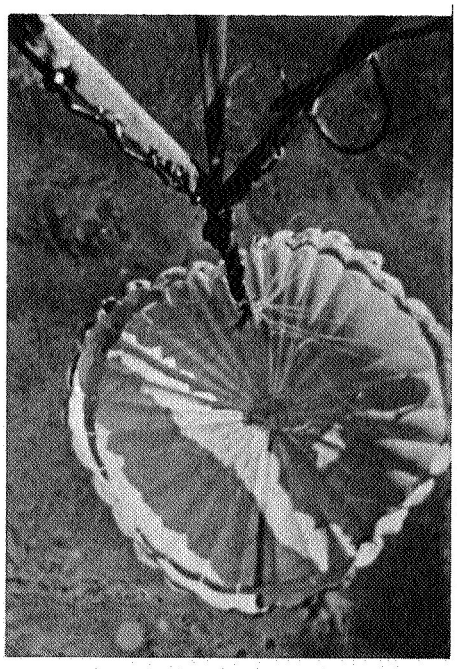

t' = 5.14 seconds

(c) Continued.

L-68-5633

Figure 12.- Continued.

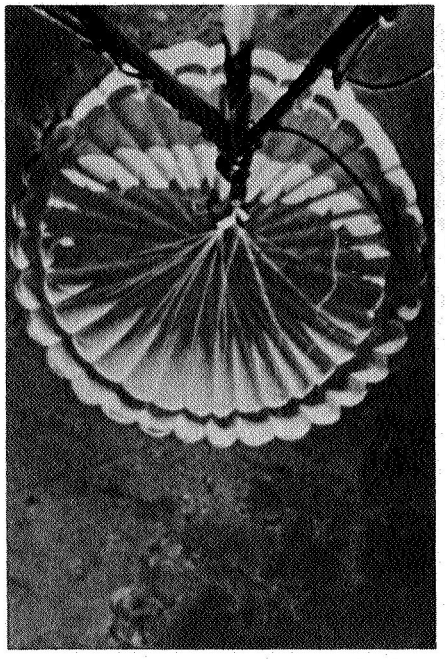

t' = 7.14 seconds

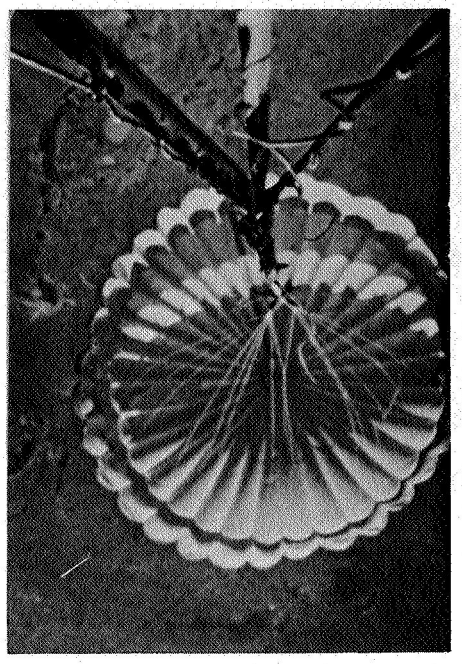

t' = 7.40 seconds

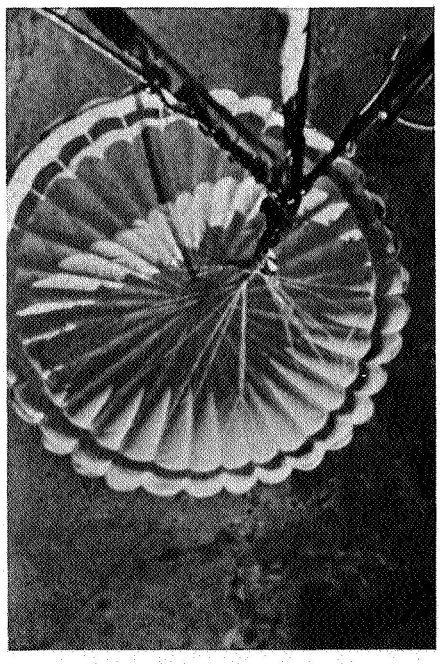

t' = 7.60 seconds

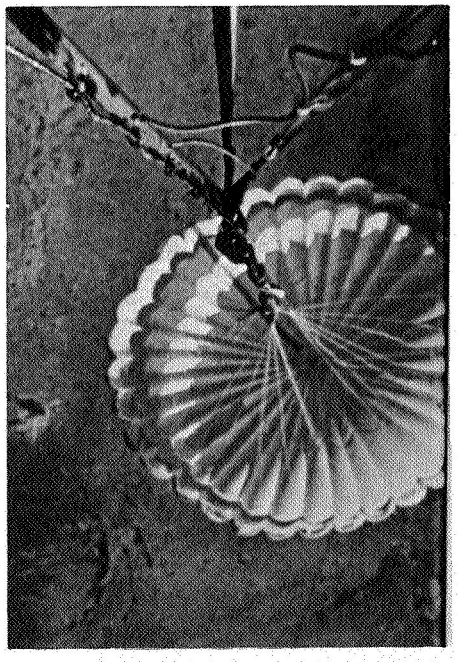

t' = 7.86 seconds

(c) Concluded.

L-68-5634

Figure 12.- Continued.

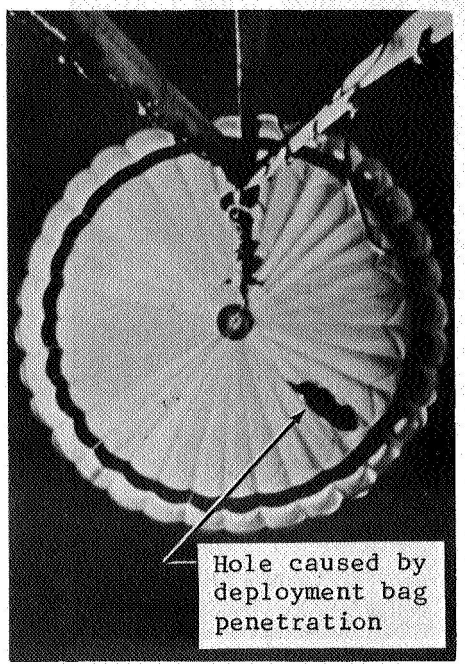

t' = 34.77 seconds

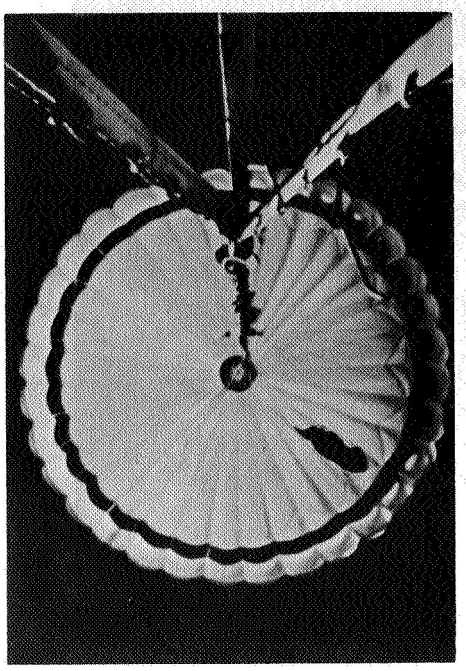

t' = 34.78 seconds

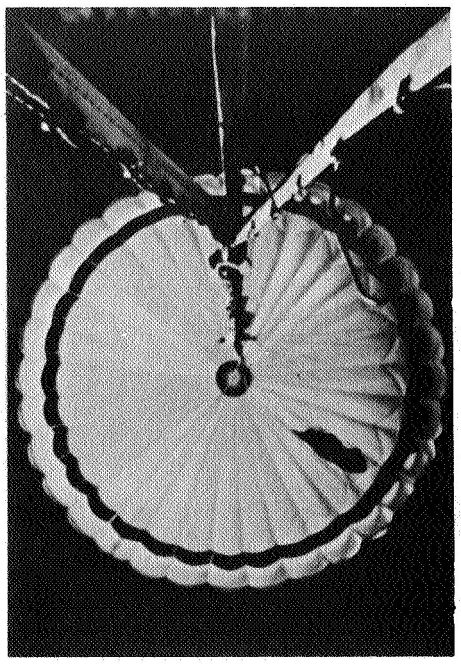

t' = 34.80 seconds

t' = 34.82 seconds

(d) Parachute near apogee.

L-68-5635

Figure 12.- Concluded.

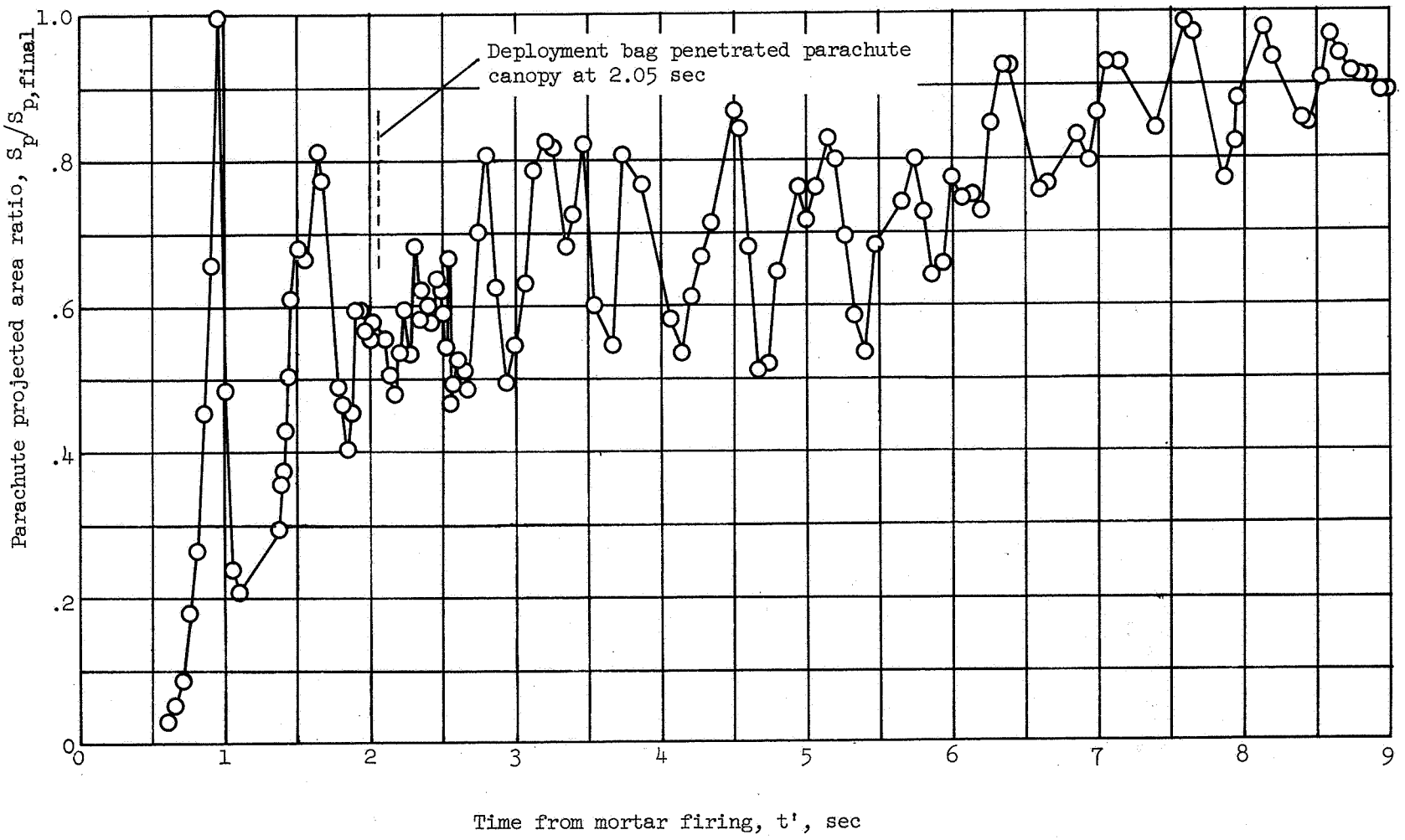

Figure 13.- Time history of parachute projected area ratio.

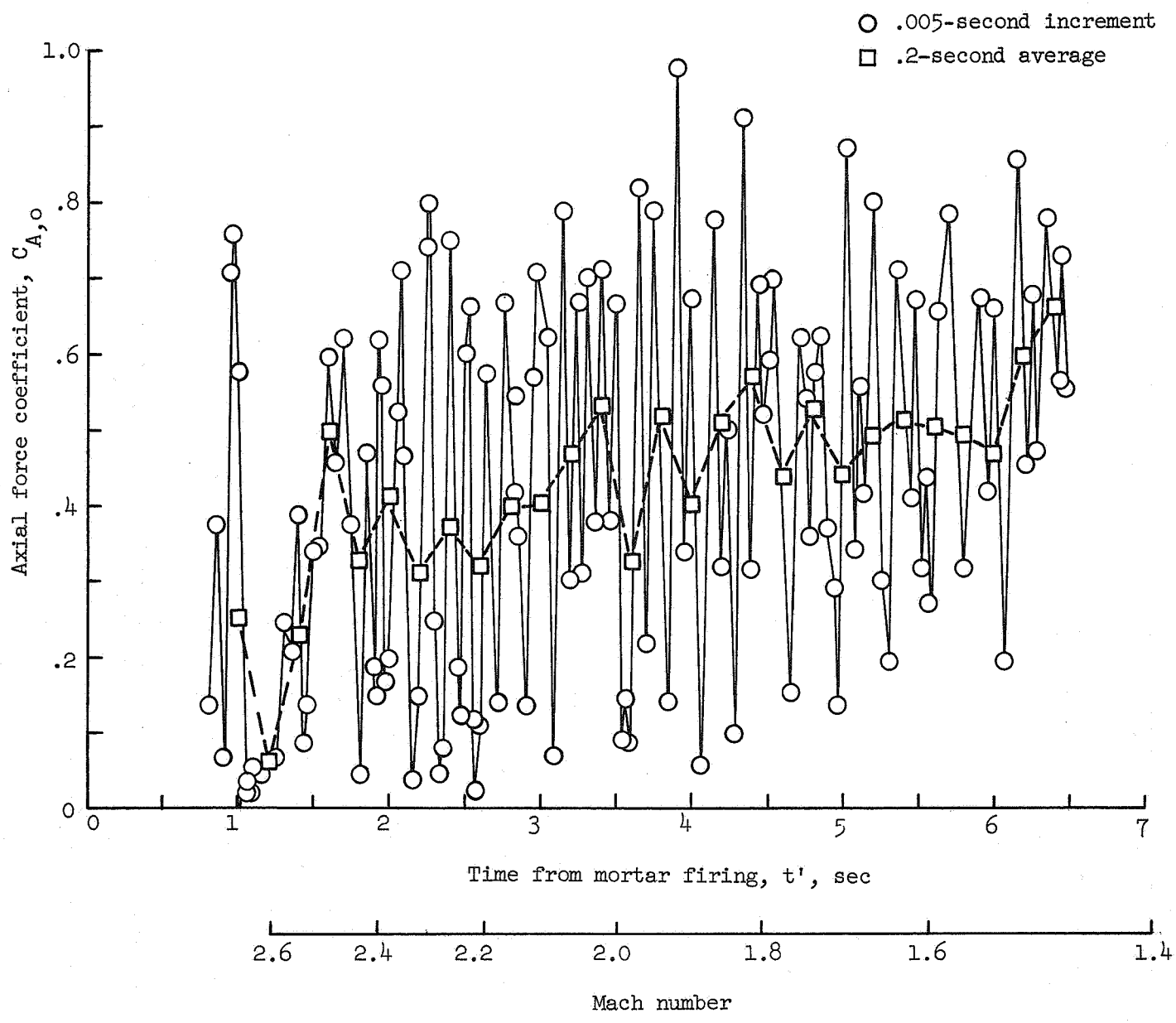

Figure 14.- Variation of derived nominal axial-force coefficient with time and Mach number.

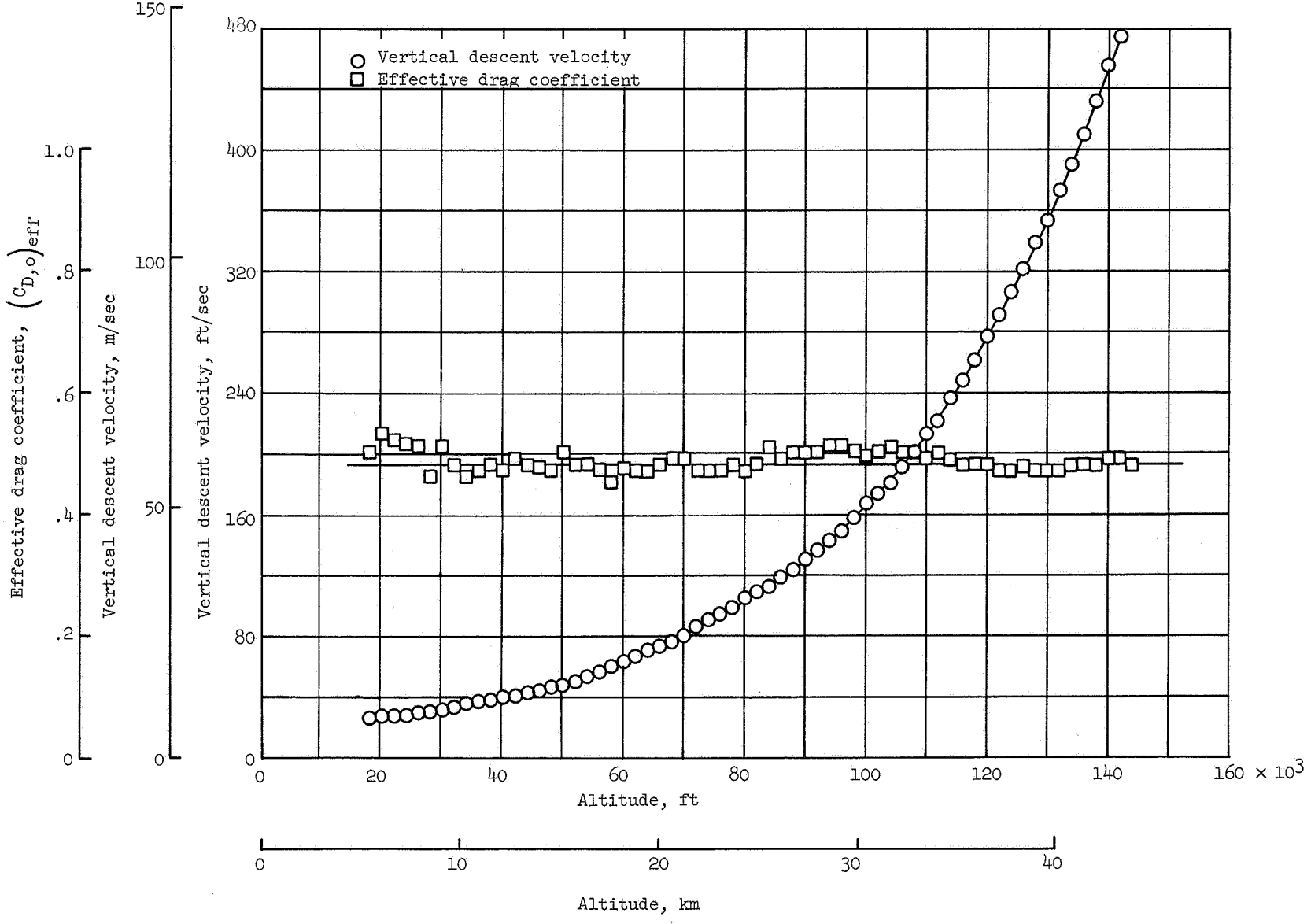

Figure 15.- Variation of vertical descent velocity and effective nominal drag coefficient with altitude.

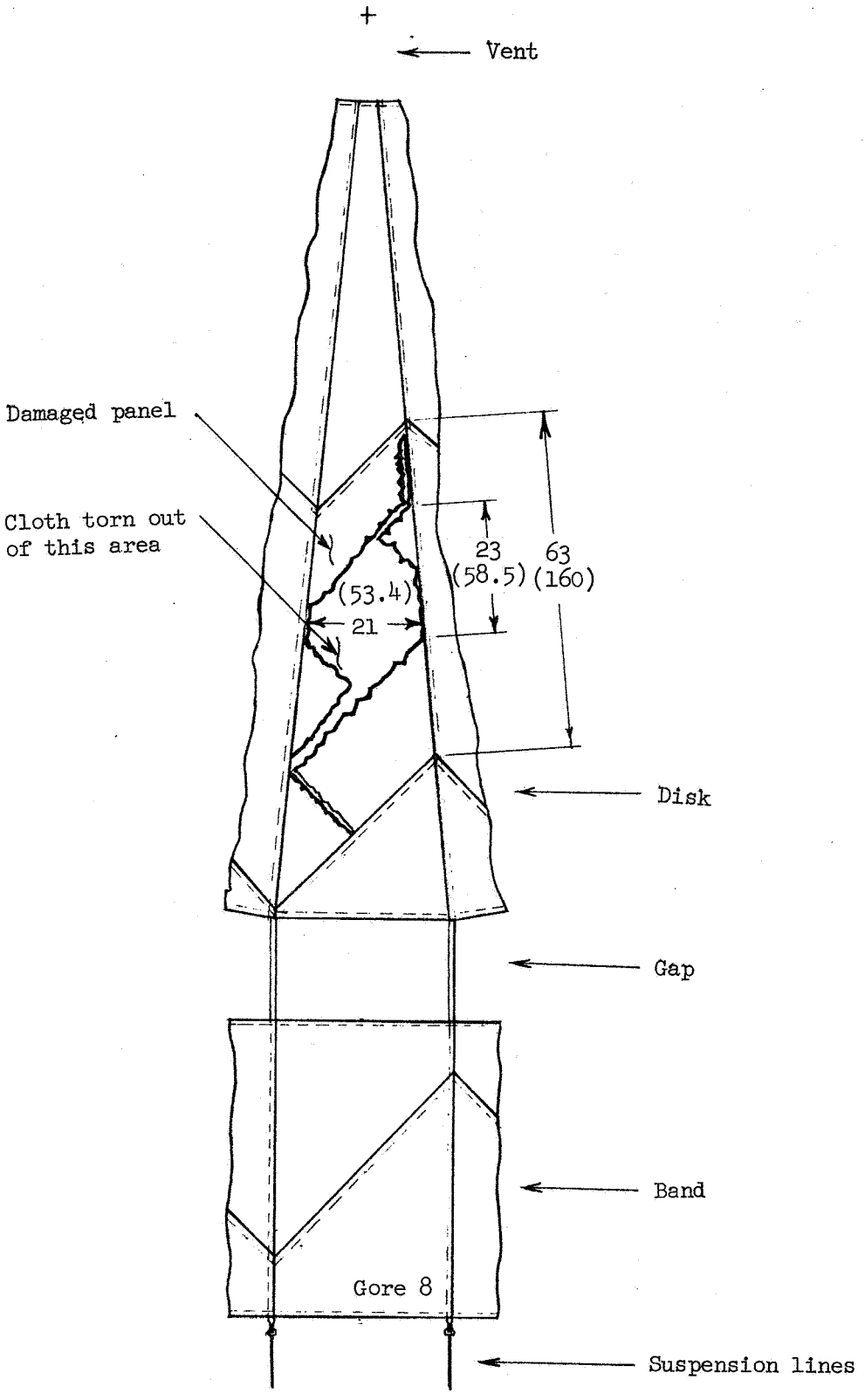

Figure 16.- Parachute damage from deployment bag penetration. Dimensions are in inches (centimeters).

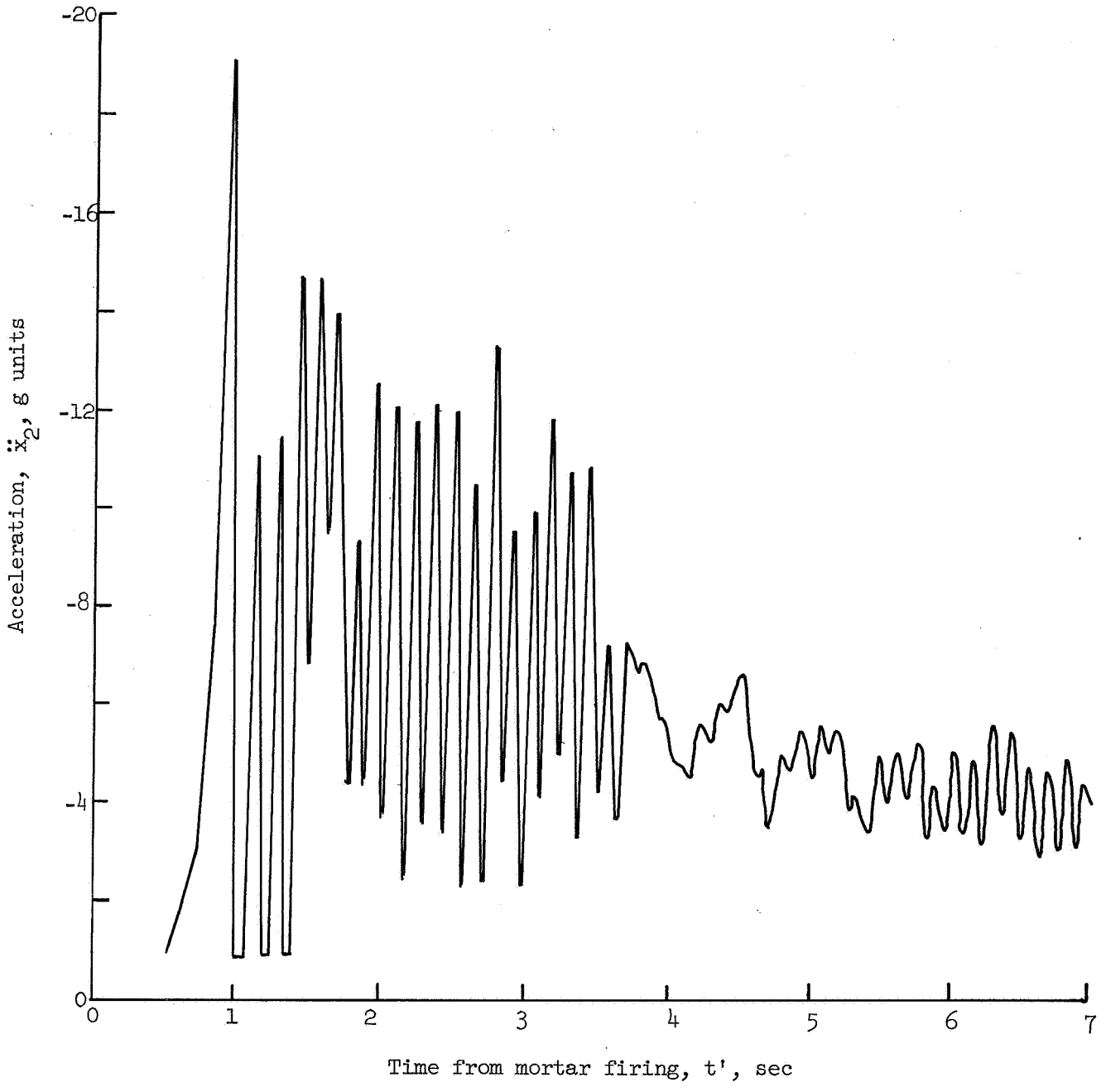

Figure 17.- Simulated payload acceleration time history.

A motion-picture film supplement L-1006 is available on loan. Requests will be filled in the order received. You will be notified of the approximate date scheduled.

The film $\left(16 \text{ mm}, 3\frac{1}{2} \text{ min}, \text{color}, \text{silent}\right)$ shows the parachute during deployment, inflation, the deceleration period, and a portion of descent as taken by a camera mounted on the aft end of the payload.

Requests for the film should be addressed to:

Chief, Photographic Division
NASA Langley Research Center
Langley Station
Hampton, Va. 23365

CUT

Date_____

Please send, on loan, copy of film supplement L-1006 to TM X-1623.

_____
Name of organization

_____
Street number

_____
City and State Zip code

Attention: Mr._____
Title_____

CUT

Place
Stamp
Here

Chief, Photographic Division
NASA Langley Research Center
Langley Station
Hampton, Va. 23365